THE EFFECTS OF Cu-, Sn-, V-, AND Ti- UNDERLAYS ON THE STABILITY OF GOLD THIN FILMS DURING ISOTHERMAL ANNEALING

By

JIN YOUNG KIM

A DISSERTATION PRESENTED TO THE GRADUATE SCHOOL
OF THE UNIVERSITY OF FLORIDA IN PARTIAL FULFILLMENT
OF THE REQUIREMENTS FOR THE DEGREE OF
DOCTOR OF PHILOSOPHY

UNIVERSITY OF FLORIDA

1988

UF LIBRARIES

ACKNOWLEDGEMENTS

The author is indebted to Dr. R. E. Hummel for his constant support and his advice during the research leading to this dissertation. His encouragement and teaching throughout the study facilitated the author's overall development as a scientist.

The author gratefully acknowledges valuable comments, suggestions and advice by Dr. R. T. DeHoff. Our discussions afforded the author a creative evolution of the research.

Lucid and enlightening comments by Dr. P. H. Holloway are gratefully acknowledged. His priceless suggestions served as a stepping-stone leading to this dissertation.

Many thanks go to all the members of the dissertation committee for their time and efforts.

My wife Eun Jin and daughter Haney are thanked for their unending patience and emotional support during the study. Thanks also go to my parents for their encouragement, without which I could not have done this.

Special thanks go to Eric Lambers for his assistance in obtaining AES spectra.

Finally, the author gratefully acknowledges the financial support by ARO (Metallurgy and Materials Science Division) and the assistance of analytical instruments by MAIC at the University of Florida.

TABLE OF CONTENTS

Page
ACKNOWLEDGEMENTS ii
ABSTRACT vi
CHAPTER 1 INTRODUCTION 1
CHAPTER 2. THEORETICAL BACKGROUND 6
2.1 Grain Growth 6
2.1.1. Grain Growth in a Single Phase Metals and Alloys. 7
2.1.2. Grain Growth in the Presence of a Second Phase 8
2.2. Thermal Stress in Thin Films 10
2.3 Stress Relaxation in Thin Films 12
2.3.1 Diffusional Creep 13
2.3.2. Mass Transport by Diffusional Creep in Thin Films. 16
2.4 Brief Survey of Hole Formation in Thin Films. 16
2.5 Brief Survey of Hillock Formation in Thin Films. 19
CHAPTER 3 EXPERIMENTAL PROCEDURE. 22
3.1 Film Preparation 22
3.2 Isothermal Annealing. 26
3.3 Film Characterization 27
3.3.1 Scanning Electron Microscopy 27
3.3.2 Transmission Electron Microscopy 27
3.3.3 Auger Electron Spectroscopy 27
3.3.4 X-ray Photoelectron Spectroscopy 29
3.3.5 X-ray Diffraction 29
CHAPTER 4. RESULTS AND DISCUSSION 30
4.1 Au/Cu Composite Films. 30
4.1.1 Formation of Holes in Gold Films During Annealing 30
4.1.1.1 Surface Topography 30
4.1.1.2 Lateral Distribution of Chemistry Near the Holes. 33

- 4.1.2 Formation of Copper Oxide During Annealing 49
- 4.1.3 Distribution of Copper Throughout the Film 54
- 4.1.4 Grain Structure of Gold 54
- 4.1.5 Fiber Texture (Preferred Orientation) of Gold 59
- 4.1.6 Kinetic Study on the Formation of Holes in Au/Cu composite Films 61

4.2 Au/Sn Composite Films 64
- 4.2.1 Surface Topography 64
- 4.2.2. Chemical State of Tin in As-deposited Au/Sn Composite Films 64
- 4.2.3 Formation of Tin Oxide During Annealing 71
- 4.2.4 Identification of Oxide of Tin 71
- 4.2.5 Distribution of Tin Throughout the Film 78
- 4.2.6 Grain Structure of Gold 83
- 4.2.7 Fiber Texture (Preferred Orientation) of Gold 83

4.3 Au/V Composite Films 92
- 4.3.1 Surface Topography 92
- 4.3.2 Formation of Vanadium Oxide During Annealing 98
- 4.3.3 Distribution of Vanadium Throughout the Film 104
- 4.3.4 Grain Structure of Gold 105
- 4.3.5 Fiber Texture (Preferred Orientation) of Gold 105

4.4 Au/Ti Composite Films 112
- 4.4.1 Formation of Gold Hillocks During Annealing 112
  - 4.4.1.1 Surface Topography 112
  - 4.4.1.2 Lateral Distribution of Chemistry Near the Hillocks 118
- 4.4.2 Formation of Titanium Oxide During Annealing 120
- 4.4.3 Distribution of Titanium Throughout the Film 127
- 4.4.4 Grain Structure of Gold 130
- 4.4.5 Fiber Texture (Preferred Orientation) of Gold 130

4.5 Summary 135
- 4.5.1 Oxides 135
- 4.5.2 Grain Growth 135
- 4.5.3 Surface Topography 137
- 4.5.4 Film Texture (Preferred Orientation) 137

4.5.5 Evolution of Microstructure 141

CHAPTER 5 FURTHER DISCUSSIONS 144
- 5.1 Formation of Holes and Hillocks in Gold Composite Films 144
  - 5.1.1 Thermal Stress in Gold Films Induced by Metal Underlays During Annealing 144
  - 5.1.2. Volume Change due to the Formation of Oxides of the Underlay Metals 151
  - 5.1.3 Surface Energy 157
  - 5.1.4 Oxidation Tendency of the Underlay Metals 159

CHAPTER 6. CONCLUSIONS 163

REFERENCES 167

BIOGRAPHICAL SKETCH 176

Abstract of Dissertation Presented to the Graduate School
of the University of Florida in Partial Fulfillment of the
Requirements for the Degree of Doctor of Philosophy

THE EFFECTS OF Cu-, Sn-, V-, AND Ti- UNDERLAYS ON THE STABILITY OF GOLD THIN FILMS DURING ISOTHERMAL ANNEALING

By

JIN YOUNG KIM

DECEMBER 1988

Chairman Rolf E. Hummel
Major Department Materials Science and Engineering

Metal underlays can be used for increasing the reliability of gold thin film metallizations. These metal underlays significantly influence the stability of gold metallizations in microelectronic circuits. They may cause failures during fabrication and during operation of a device. The effects of metal underlays on the stability of gold thin films during isothermal annealing have been investigated. Cu-, Sn-, V-, and Ti- underlays of 130 Å thickness were sandwiched between quartz substrate and gold films of 750 Å thickness by thermal evaporation in a high vacuum. Isothermal annealing was carried out in a tube furnace at 300 °C, 400 °C, and 500 °C for 1 hour in air. Following heat treatment the topography of the film surface, the internal grain structure, the composition profiles throughout the film thickness, the lateral distribution of chemistry across the film surface, the chemical reactions during annealing, and the film texture were examined using scanning

electron microscopy (SEM) with capabilities for energy dispersive X-ray spectroscopy (EDS) and backscattered electron (BE) image, transmission electron microscopy (TEM), Auger electron spectroscopy (AES), scanning Auger microscopy (SAM), X-ray photoelectron spectroscopy (XPS), selected area diffraction (SAD) in TEM and x-ray diffraction. It was found that (1) Cu-, Sn-, V-, and Ti- underlays sandwiched between gold thin films and substrate form oxides (CuO, SnO_2, V_2O_5 and TiO_2 respectively) on the free surface of gold and along the grain boundaries of the gold films during annealing in air; (2) Ti underlays which have a strong tendency towards oxidation prevent grain growth of gold during annealing as stated above, while Cu underlays which have a small tendency towards oxidation do not prevent grain growth of gold during annealing; (3) Au/Sn composite films show a rough surface structure in both, as-deposited and annealed composite films. The surface roughness of Au/Sn composite films results from the rough surface structure of the Sn underlays. Au/Sn composite films form neither hillocks nor holes during annealing in air. (4) Lastly, it is believed that the formation of holes in Au/Cu composite films and the formation of hillocks in Au/V and Au/Ti composite films are caused by an interplay between stress relaxation, capillarity force, and oxidation behavior of the underlay metals.

Additionally, the critical factors of metal underlays for the reliability of gold metallizations have been found to be as follows: (A) Oxidation tendency of metal underlays, (B) Thermal stress due to the difference in thermal expansion coefficients, (C) Volume change due to the formation of oxides of the underlay metals and (D) Surface energy.

CHAPTER 1
INTRODUCTION

With the continuing size reduction and complexity of integrated circuits, the stability (reliability) of microelectronic devices is becoming more important. One of the problems awaiting solution is the failures in thin film metallizations. Metallization is the metal interconnections between individual electronic components such as transistors in a microelectronic chip. The stability of metallizations will become increasingly important in the continuing evolution of the market to very large scale integrated (VLSI) circuits with low micrometer to submicron features [1-12].

A variety of thin film metallizations are currently used in the IC industry. Metallizations generally require a good conductivity, electromigration resistance, corrosion resistance, adherence, and bondability, etc [3, 11-14]. Although no single metal can satisfy all requirements for IC technology, aluminum metallizations have found widespread use in the IC industry because of their compatibility and cost effectiveness [3, 10-11]. As the line width approaches to a micron or less, however, the much lower electromigration (EM) failure rate of the gold metallization may force a switch from aluminum to gold [3, 10-11].

The "median time to failure" (t_{50}), a parameter which indicates the time at which 50 % of a large number of identical test stripes have failed, is commonly expressed by the Black-equation [15],

$$t_{50} = A\, j^{-n} \exp(Q/kT)$$

where A is a constant which contains structural parameters such as film geometry and microstructure, j is the current density, n is a numerical value which is about 1.5, Q is the activation energy, k is the Boltzman constant, and T is the temperature. The lifetime of a device is seen to increase exponentially with increasing Q. The activation energy in gold films is twice as large as that in aluminum films (Q = 0.4 eV for pure Al, 0.98 eV for Au, and about 0.44-0.77 eV for Al with Cu and Si) [3,7,16]. Corrosion resistance in severe environments is an additional advantage of a gold metallization.

In gold metallizations, a metal underlay is required to provide good bonding to the substrate because gold does not readily adhere to oxide or oxidized substrates commonly used for microelectronic circuits and tends to ball up during heat treatment even below the melting point [11,17-18]. These metal underlays, however, significantly influence the stability of gold films during fabrication and during operation of a device.

The present annealing study of thin gold films provides the basis for understanding the chemical reactions which may occur during fabrication and during operation of a device. An annealing study simplifies the failure mechanisms (i.e., thermally activated failures which can occur without currents passing through the device) in thin film metallizations. In the last several years it has become quite apparent that the thermally activated failures can be critical for the reliability of microelectronic circuits. It was noted in a recent issue of "Science News" that a thermally activated process such as the formation of holes by stress relief will be one of the major concerns of today's fastest chips and for the next generation of chips [19].

As an example, Hummel et al. have shown that alkali metals cause thin gold films to disintegrate into unconnected islands when heated, while indium underlays between gold and quartz substrate prevented thermal grooving in Au films [4-5, 10]. It was concluded that In_2O_3 which formed on the free surface of gold prevented thermal grooving during heat treating in air by limiting the mass transport process. It has also been reported that thin Au films on Ni underlays deposited onto oxidized silicon wafers form "porosity" after heating between 250 °C and 450 °C in oxidizing ambients [13 14]. It was noted that a porous, discontinuous thin Au film was thermodynamically stable by considering a model which involves grain boundary grooving.

The objective of this dissertation is to investigate the influence of various metal underlays on the stability of gold thin films during isothermal annealing and to obtain a better understanding of the mechanisms involved.

In order to achieve this objective, Cu-, Sn-, V-, and Ti- underlays have been chosen based on the standard free energy for oxide formation as a function of temperature (Richardson's chart, Figure 1. [20]). For film preparation, Cu-, Sn-, V-, and Ti underlays of about 130 Å thickness were sandwiched between quartz substrate and gold films of about 750 Å thickness by thermal evaporation in a high vacuum. Isothermal annealing was carried out in a tube furnace at 300 °C, 400 °C and 500 °C for 1 hour in air. Following heat treatment, the topography of the film surface was characterized in a routine fashion using SEM with capabilities for EDS

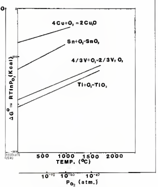

Figure 1. Standard free energy of formation of oxides as a function of temperature [from ref. 20]

and B.E. image. Transmission electron microscopy (TEM) was used to determine the internal grain size and grain structure. AES, Auger sputter profiling, SAM, XPS, and SAD in TEM were employed to determine the chemical composition of the film surface and throughout the film thickness, the lateral distribution of chemistry across the film surface, and the chemical reactions during annealing. The texture of the gold films was characterized using x-ray diffraction.

The effects of metal underlays on the stability of gold thin films during isothermal annealing will be shown in terms of (1) oxide formation of the underlay metals, (2) grain growth of gold (3) formation of holes/hillocks, (4) surface structure, and (5) preferred orientation of gold. The critical factors of metal underlays for the reliability of gold metallizations have been found to be as follows (A) Oxidation tendency of metal underlays, (B) Thermal stress due to the difference in thermal expansion coefficients (C) Volume change due to the formation of oxides of the underlay metals, and (D) Surface energy.

CHAPTER 2
THEORETICAL BACKGROUND

2.1 Grain Growth

A random grain structure in a polycrystal is inherently unstable and, upon annealing at high temperature (≥ about 0.5 Tm), any possible unbalanced forces will cause a grain boundary to move towards its center of curvature [21-22]. As a consequence, some of the grains grow, but others shrink and vanish. If a grain has six boundaries it will be in a metastable equilibrium. However, if a grain has less than six boundaries, it will shrink and eventually disappear during annealing. On the other hand, lager grains which have more than six boundaries will grow [21]. Because the volume of the specimen is constant, the number of grains decreases and thereby the mean grain size increases as a consequence of such boundary migration. This phenomenon is known as grain growth or grain coarsening [21-22].

The driving force for grain growth is the boundary free energy [22]. A curved boundary creates a difference in free energy (ΔG) that drives the atoms across the boundary. In a pure metal ΔG is given by [21]

$$\Delta G = 2\gamma V_m / r$$

where r = the radius of curvature

γ = the grain boundary energy

V_m = the molar volume.

The pulling force per unit area of boundary (F) is given by [21]

$$F = \Delta G/V_m$$

Thus the force on a boundary is simply the free energy difference per unit volume of material

2.1.1 Grain Growth in a Single Phase Metals and Alloys

In pure metals and in single-phase alloys the rate at which the mean grain diameter **D** increases with time will depend on the grain boundary mobility and the driving force for boundary migration If we assume that the mean radius of curvature of all the grain boundaries is proportional to the mean grain diameter **D**, the velocity of grain boundary migration (v) will be given by [21]

$$v = \alpha M (2\gamma/D)$$

where α = a proportionality constant,

M = the grain boundary mobility,

γ = the grain boundary energy and

D = the mean grain diameter

Experimentally the grain growth obeys a relationship of the form [21 22]

$$D = k\,t^n$$

where t is the annealing time; k and n are proportional constants which depend on the material and the temperature The value of n the time exponent in isothermal growth is usually much less than 0.5 or at most equal to 0.5 [20-21]

2.1.2 Grain Growth in the Presence of a Second Phase

Figure 2 depicts the effect of a spherical particle on the grain boundary migration. The moving boundaries are thought to be attached to the particles so that the particles exert a pulling force on the boundary restricting its motion [21]. The free energies (G) at P_1, P_2, and P_3 are given as

$$G_1 = G_3 = A\gamma_b + 4\pi r^2\gamma_s$$

$$G_2 = (A - \pi r^2)\gamma_b + 4\pi r^2\gamma_s$$

where A = the area of grain boundary

r = the radius of a particle

γ_b = the area of grain boundary

γ_s = the surface energy of a particle.

When the boundary moves from P_1 to P_2 in Figure 2, the difference in free energy ($\Delta G_{1\rightarrow 2}$) becomes $-\pi r^2\gamma_b$ (< 0) and therefore the grain boundary migration is favorable. However, when the grain boundary moves from P_2 to P_3 in Figure 2, the difference in free energy ($\Delta G_{2\rightarrow 3}$) becomes $\pi r^2\gamma_b$ (> 0) and therfore the grain boundary migration is unfavorable. Thus the grain growth is restrained in the presence of a second phase. This is called "pinning effect" of a second phase on the grain boundary migration [21].

The above type of grain growth is refered to as normal (or continuous grain growth) [21]. In contrast to this, abnormal grain growth (or secondary recrystallization or discontinuous grain growth) can occur when normal grain growth is inhibited due to the presence of a fine precipitate array and when the temperature is high enough to allow a few special grains to overcome the inhibiting force and to grow disproportionately [21].

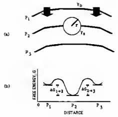

Figure 2 (a) The effect of spherical particles on grain boundary migration
(b) The free energy (G) at P_1, P_2 and P_3.

2.2 Thermal Stress in Thin Films

When a thin film is grown on a relatively thick substrate and then heated to a temperature that is different from its temperature during deposition, a thermal stress will be introduced due to the differences in the thermal expansion coefficients of the film and the substrate material

The thermal stress can be calculated by considering two different samples of equal shape and of initial length, l. It is assumed that (a) there is a biaxial system of stress in the sample, (b) an equal stress model can be applied, (c) the isotropic elasticity theory is valid, and (d) the samples are bonded at their common interface. When the samples are heated to a temperature Ta the length l_1' and l_2' (Figure 3) will be given by (private communication with F. Ebrahimi)

$l_1' = l + \alpha_1\Delta T + (\sigma_{xx} - \nu\sigma_{yy})/E_1$

$l_2' = l + \alpha_2\Delta T - (\sigma_{xx} - \nu\sigma_{yy})/E_2$

where α_1, α_2 = the thermal expansion coefficients of the samples

E_1, E_2 = the Young's moduli of the samples

ν = the Poisson's ratio

$\Delta T = Ta - Ts$ where Ts = the initial temperature

When the samples are isotropic and bonded at their interface, one can write $\sigma_{xx} = \sigma_{yy}$ (= σ_{th}) and $l_1' = l_2'$. Therefore the thermal stress, σ_{th}, that makes the length of the samples equal when heated will be given by

$\sigma_{th} = \{E_1E_2/(1-\nu)(E_1 + E_2)\}(\alpha_1 - \alpha_2)\Delta T$

A positive value of σ_{th} corresponds to a tensile stress

If the thermal stress induced in the substrate by the thin film is negligible, then

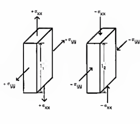

Figure 3: A biaxial system of thermal stress acting on the two different samples of equal shape

l_f' (for the film) $= l + \alpha_f \Delta T + (\sigma_{xx} - \nu\sigma_{yy})/E_f$

l_s' (for the substrate) $= l + \alpha_s \Delta T$.

It is assumed that the film is again isotropic and bonded at the interface, which yields $\sigma_{xx} = \sigma_{yy}$ (= σ_{th}) and $l_f' = l_s'$. Therefore the thermal stress σ_{th} due to the constraint imposed by the film/substrate bonding is given by [23-26]

$$\sigma_{th} = [E_f/(1-\nu)](\alpha_f - \alpha_s)(T_s - T_a)$$

where E_f = Young's modulus

ν = Poisson's ratio,

α_f = thermal expansion coefficient for the film,

α_s = thermal expansion coefficient for the substrate,

T_a = temperature at measurement,

T_s = temperature of the substrate during film deposition.

A positive value of σ_{th} corresponds to a tensile stress in the film.

2.3 Stress Relaxation in Thin Films

It is generally known that thin films condensed onto substrates are, unlike bulk materials, in a non-equilibrium state which is characterized by a high level of stress [25, 27-29]. The total stress in a film consists of two major components, (1) a "thermal stress" arising from the difference in the thermal expansion coefficients of the film and the substrate, and (2) an "intrinsic stress" resulting from the structure and growth of films [27]. The tendency of a thin film towards equilibrium brings about a stress relaxation in the film [28]. It can take place during heat treatment or even during long time storage at room temperature [19, 28].

Stress relaxation in thin films is different from bulk materials not only due to the relatively small dimensions of the film but also, frequently, due to the presence of a constraining substrate [30-31]. When a thin film is stressed by an amount smaller than the elastic limit, it deforms elastically and returns to its original shape after the stress is relieved. However, when the stress is beyond the elastic limit, the film deforms plastically, that is, it does not return to the original shape after the stress is relieved [32-33]. This plastic deformation usually leads to the formation of hillocks (protrusions) or holes in the films [28, 30-31, 33-34]. They are, of course detrimental during the performance of a microelectronic device, causing electrical shorts and opens in integrated circuits.

The stress relaxation mechanism strongly depends on the film deposition technique (grain size, texture, interface structure) and conditions (defects and composition) [29, 33].

2.3.1 Diffusional creep

A diffusion induced flow of matter can be caused by migration of vacancies between differently stressed boundaries in a polycrystalline solid [35-37]. In the absence of pressure gradients, the flux of atoms, due to migration of lattice vacancies or interstitial atoms will be proportional to the gradient of the concentration of these lattice defects. In the presence of pressure gradients, however, it tends to be energetically advantageous to move the lattice defects in whichever direction will relieve the inequality of pressure [35]. Figure 4 shows a schematic representation of vacancy flow within a grain experiencing tensile stress [33]. The atom flow will be opposite to the vacancy flow causing the grain to elongate in the direction of tensile stress.

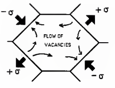

Figure 4. Schematic of vacancy flow within a grain experiencing tensile stress [from ref. 33].

The diffusion flow resulted from the flow of point defects (usually vacancies) through grains under a concentration gradient generated by the applied stress is called Nabarro-Herring creep [35-38] and that from the flow of point defects (usually vacancies) round their boundaries is called Coble creep [36, 38]. In a thin polycrystalline film in tension the stress relaxation rate by Nabarro-Herring creep is given by [37, 39]

$d\sigma/dt = \{(-B_n\Omega M D_l)/(ghkTf)\}\sigma$

where $d\sigma/dt$ = stress rate

M = elastic modulus

Ω = atomic volume

B_n = geometrical factor ≈ 10

g = grain size

h = film thickness

D_l = lattice diffusion coefficient

f = correlation factor for diffusion

k = Boltzmann constant

T = absolute temperature

σ = stress.

The stress relaxation rate by Coble creep is given by [37-39]

$d\sigma/dt = \{(-B_1\Omega M D_g\delta)/(gh^2kT)\}\sigma$

where B_1 = geometrical factor ≈ 15

$D_g\delta$ = the combined grain boundary diffusion parameter.

The driving force for diffusional creep was shown to result from a change in equilibrium vacancy concentration with stress [35-37]. When a normal tensile stress acts across a grain boundary the increase in vacancy concentration is given by [36-37],

$$\Delta C = C_0 \sigma_n \Omega / kT$$

where ΔC = the change in vacancy concentration,

C_0 = the equilibrium vacancy concentration at temperature T in a stress-free crystal,

σ_n = the component of the local stress normal to the boundary,

Ω = the atomic volume.

2.3.2. Mass Transport by Diffusional Creep in Thin Films

Figures 5a and 5b [25] show schematically the mass transports by diffusional creep in a polycrystalline film containing elastic strains. It is assumed that all areas of the free surface of a film are equally efficient sources and sinks of vacancies. For a tensile stress in a film, the mass transport occurs from the free surface into the interior and for a compressive stress it occurs from the interior onto the free surface of a film. When allowing localized areas to be more efficient than the remaining areas, the mass transport by diffusional creep can lead to the formation of hillocks or holes on a film surface [25]. The localized areas can be holes or cracks in an oxide layer (or film with low diffusion rates) on a film, or selected diffusion paths where diffusion rates are high compared with the rest of the film [25].

2.4 Brief Survey of Hole Formation in Thin Films

Hole formation during annealing has been reported in various thin films under a wide range of conditions. The mechanisms proposed for hole formation in thin films are mainly thermal grooving (also called grain boundary grooving) [2-5, 10,

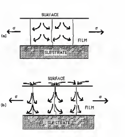

Figure 5 Schematic representation of mass transport by diffusional creep in a film [from ref 25]
(a) Volume diffusion is dominant.
(b) Grain boundary diffusion is dominant

13-14, 40-41], diffusional creep [25, 33-34, 42], annihilation of excess vacancies [43-50], surface diffusion [51-53], and Kirkendall voids in thin films [54-62].

Thermal grooving is caused by a mass transport due to an imbalance of surface tension where the grain boundary intercepts the free surface [3-5, 10]. Hummel et al. have suggested that the holes in thin gold films are formed by thermal grooving when heat-treated at uniform temperatures in a furnace [3-5, 10]. They also have shown that thermal grooving was accelerated by alkali metals in a gold film while it was prevented by indium underlays between gold and quartz substrate [4-5, 10]. It was proposed by Srolovitz et al. using an equilibrium argument that polycrystalline films were unstable due to the presence of grain boundary vertices, which might lead to hole formation and growth [40-41]. It has been shown by Chao et al. that considering Srolovitz and Safran's model of grain boundary grooving, a porous and discontinuous thin Au film is thermodynamically stable in thin Ni/Au metallizations after heating [13]. They also suggested that stress in thin films might cause a greater pore size than the equilibrium pore size.

It was recently reported by Groothuis et al. that stress relaxation by diffusional creep in the bulk or in grain boundaries was the dominant mechanism for the formation of voids in Al-Si interconnects during heat treatment [33-34]. Chaudhari considered diffusional creep as the growth mechanism for both annealing hillocks and depressions [25]. Brinkman proposed a mechanism of pore formation by which the presence of tensile stress might affect the nucleation and growth of voids [63]. Yue et al. reported the formation of stress induced voids in Al based interconnects during IC wafer processing [42]. Besides, stress induced grain boundary fractures [64] and stress induced void formations [65] were reported by other investigators in Al-Si interconnects.

Lloyd and Nakahara [43-48] have suggested that void growth in evaporated gold film in the absence of electromigration occurs as a result of annihilation of excess vacancies trapped in the film during deposition at pre-existing voids. Sharma and Spitz have suggested that a high density of voids observed in silver films on room temperature aging and high temperature annealing was caused as a result of accumulation of vacancies at sinks such as the pre-existing voids or other vacancies in the as-deposited films [49, 50].

It has been reported that Kirkendall voids are formed in a diffusion couple of components A and B at the side of the fast diffusing species during interdiffusion, if the bulk diffusivities $D_A >> D_B$ [54, 66]. The Kirkendall voids have been observed in thin film couples of Pd-Sn [54], Au-Sn [55], Au-Pb [56], Pb-alloy [57], Cu-Au [58-59], and Cu-Ni [60].

Besides, holes were observed to develop in thin gold films on, or sandwiched between two evaporated layers of either zinc sulfide or cadmium sulfide [67], in nickel and gold films [68], in electro deposited gold-cobalt [69], and gold-nickel [70] films under a various conditions.

2.4 Brief Survey of Hillock Formation in Thin Films

Surface hillock formation during annealing has been reported in thin films of various metals. Hillocks grow extensively in Al [29, 71-74], Au [75-76], Sn [30-31], Pb [30-31, 72, 77-79], Ag [24, 51, 80], Pb in Au-alloy [81], Cu/Sn [82], and Au/$W_{75}C_{25}$ [83] films during annealing.

Several mechanisms have been proposed to explain the growth of these hillocks. Although the mechanism of hillock growth has not yet been fully elucidated, it has been generally agreed that hillock growth in thin films is associated with a stress relaxation phenomenon [28-31, 71-73, 77]. Mechanisms such as diffusion creep [25, 28-29, 71-73, 77, 79-80], grain boundary sliding [25, 71, 77], grain growth [84-85], dislocation slip [86], recrystallization [75], and impurity atoms [76] have been proposed to explain the growth of hillocks.

Hershkovitz et al. reported that the appearance of hillocks on the surface of thin aluminum films deposited by electron beam evaporation was an indication of diffusion during the temperature cycle and the predominant stress relaxation mechanism was grain boundary diffusion creep [29]. Chaudhari suggested that a difference in chemical potential of vacancies between the region in compression and the region in tension leads to mass flow towards the region in a tensile stress [30-31]. It was reported by Chaudhari [30-31] that hillock growth is favored when $\gamma \leq \sigma d/2$ (where σ is the compressive stress, γ is the surface energy of the film and d was the size of the local area in tension). Inserting a typical values for γ (of the order of 0.1 - 0.5 J/m^2) and for d ($\approx 10^{-6}$ m) into the above equation, then the value of σ is about (0.2-1.0) x 10^6 N/m^2 [30-31]. This is a relatively low value of stress for films subjected differential thermal stress and therefore hillock growth is expected to be the favored mode of stress relaxation [30-31]. Santoro reported that hillock formation in thin aluminum films relieved some of the compressive stress present on heating [73]. It was suggested that because the mass motion causing hillock formation was not a reversible process, the stress relaxation was probably accomplished by gross thinning of the film or by grooving or separation at grain boundaries.

Grain boundary sliding can also be shown to relieve the stress in thin films [25, 71, 77]. Grain boundary sliding does not usually involve appreciable flow of material, while diffusional creep does involve the movement of material [25, 77]. Herman et al. suggested diffusional creep and grain boundary sliding mechanisms as the source of mass transport for the relief of stress which was thermally induced in Al thin films [71]. It was also reported by Lahiri that annealing hillocks in Pb films could be accounted for by grain boundary sliding as well as by diffusional creep [77].

Grain growth (or grain boundary migration) was reported to lead to stress relaxation when the film was under a compressive stress [84]. Chaudhari suggested that since the coalescing of boundaries generates a tensile stress in films, grain growth can not relax tensile stress in films [84]. It was, however, reported by Griffin et al. [85] that the overall decrease in the tensile strength of thin films of Al-1% Si was primarily due to the observed increase in grain size.

Murakami [86] found that significant strain relaxation in Pb thin films occurred by a dislocation-slip mechanism at low temperature below 50 K. It was also suggested by several investigators that at relatively high temperatures the strain was relaxed mainly by a diffusion controlled mechanism [86-87], at low temperatures the strains was primarily relaxed by a non-diffusive process such as dislocation slip or twinning [86, 88].

Pennebaker proposed that hillock growth in sputtered gold films was due to recrystallization being driven by thermal stress during annealing [75].

CHAPTER 3
EXPERIMENTAL PROCEDURE

3.1 Film Preparation

For the film preparation, Cu-, Sn-, V- and Ti underlays of about 130 Å thickness were sandwiched between quartz substrate and gold films of about 750 Å thickness by thermal evaporation in a high vacuum. This geometry of a gold film with a metal underlay will hereafter be referred to as a "gold composite film." Optically flat commercial grade polished fused quartz plates with dimensions of 2.5 x 3.5 x 0.1 cm^3 were ultrasonically cleaned for 10 - 15 minutes in Alconox detergent in de-ionized water, Microwash in de-ionized water, electronic grade acetone and finally electronic grade alcohol.

1) Alconox detergent (7.3 % phosphorous by weight; pH 9.0 - 9.5) solution was utilized to remove the gross contaminants including oils, greases, soils and carbon products followed by a rinse with de-ionized water.
2) Microwash (a general purpose labware cleaner) in de-ionized water was applied to further remove water-soluble contaminants by using a higher grade detergent followed by a rinse with de-ionized water.
3) Electronic grade acetone, a semi-polar solvent acting as a vapor degreaser was used followed by a rinse with acetone.

4) Electronic grade alcohol, a less polar solvent containing fewer inherent impurities was finally utilized to continue the cleaning action initiated by the acetone wash followed by a rinse with methanol.

The cleaned substrates were subjected to a stream of pressurized dry air and examined with the aid of an optical microscope to discard the ones exhibiting gross defects such as scratches, bubbles, and seeds. The fused quartz used are stable at temperatures up to 500 °C [89]. The impurity content is given by the manufacturer as follows:

Al_2O_3 : 60 - 100 ppm, Fe_2O_3 : 3 -5 ppm , K_2O : 3 ppm,

TiO_2 : 5 ppm, Na_2O : 4 ppm, Ca : 0.5 ppm, B : 0.3 ppm

The substrates were then placed on the sample holder in the vapor deposition vacuum chamber. Four or five substrates were loaded at the same time. The substrate-to-source distance was about 25cm.

The source materials for film production were in wire form. They had the following purity: 99.999 % for gold and copper, 99.98 % for tin and titanium, and 99.5 % for vanadium. The wire was carefully wiped clean using acetone and methanol, and placed in a tungsten boat for Ti, V, and Cu , and a molybdenum boat for Au and Sn deposition. These procedures were performed just before entry into the vacuum chamber to minimize the extent of contamination between cleaning and entry.

Prior to opening the bell jar, the system was heated by wrapped heating tapes around the chamber in order to minimize impurities adsorbed along the walls and constituent parts of the chamber. A constant stream of nitrogen was used for the same purpose, while the chamber was open. After the substrates and source materials were placed in the chamber, the system was closed and pumped down immediately.

The vacuum system consisted of a glass bell jar chamber pumped by roughing pumps (a mechanical pump and a liquid N_2 cooled adsorption pump) and a sputter-ion pump with titanium sublimators. The mechanical pump was used to bring the pressure in the chamber down to 1.5×10^{-1} Torr within 10 minutes. Near the beginning of this period, the chamber was purged by laboratory grade nitrogen in order to reduce the partial pressure of oxygen and water vapor. After the pressure was backed up to atmospheric pressure, the system was pumped down by the mechanical pump again. This process was repeated two or three times before turning on the adsoption pump.

The mechanical pump was then turned off and sealed from the bell jar by a valve. A liquid N_2-cooled adsorption pump reduced the overall pressure down to about 2×10^{-3} Torr by reducing the partial pressures of nitrogen, carbon dioxide, water vapor and residual hydrocarbons. Near the end of this step, the heating tapes around the chamber were turned off and the cooling fans were started.

After outgassing the titanium sublimator, the adsorption pump was closed off and the ion pump was started. Two sputter-ion pumps, in conjunction with the titanium sublimator, brought the system pressure down to the deposition pressure of about 5×10^{-5} Torr within 4 to 7 hours. The titanium sublimator was used at about 20 minutes intervals for 40 seconds. When the base pressures in the chamber were in the range of $4 - 8 \times 10^{-8}$ Torr, the deposition was performed.

For gold composite films, a metal underlayer of about 130 Å thickness was deposited first onto the quartz substrate by thermal evaporation using a 3 KVA power supply. A shutter was used initially to isolate the substrates from the metal source. The shutter was kept closed until the current was stabilized. After stabilization, the shutter was opened and a watch was simultaneously started for the determination of deposition rate. Upon reaching the desired thickness, the current was turned off, the shutter closed and the watch stopped. After the first deposition, about 15 to 30 minutes were required for the system to reach again the base pressure of 4 - 8 x 10^{-8} Torr for the subsequent deposition of Au without breaking the vacuum. Gold films of about 750 Å thickness were then deposited on the metal underlay-covered quartz substrate. The adhesive tape test on as-deposited gold composite films showed that interfacial contamination (oxide) did not hinder the adhesion of the gold film to the underlay metals seriously. The pressures during deposition were about 1 - 4 x 10^{-6} Torr and the deposition rates ranged from 1 to 8 Å/sec. The substrate temperature during deposition was about 45°C due to the radiation heating [90].

The mean free path is defined as the average distance traveled by a molecule between successive collisions with other molecules in the gas phase [91]. The mean free path of the gas molecules is inversly proportional to the pressure in the chamber. For air molecules at 25 °C and 1 x 10^{-6} Torr the mean free path is about 4,500 cm [92]. Thus the pressure during deposition, about 1 - 4 x 10^{-6} Torr, was low enough to ensure a straight-line path for most of the evaporated source materials, for substrate-to-source distance of 25 cm.

The thickness of the films was measured in situ with a quartz crystal thickness monitor positioned near the substrates during deposition. Since the monitor was calibrated for gold, the correction factors for the other elements were calculated and taken based on the density ratio of the metals to gold. The ion pump was turned off after completion of the deposition and the films were left in the vacuum chamber for several hours for cooldown. The films were then stored in dessicators while waiting for analysis or heat treatment.

3.2 Isothermal Annealing

Isothermal annealing was carried out in a tube furnace at 300 ^{o}C, 400 ^{o}C and 500 ^{o}C for 1 hour in air. The annealing temperatures were chosen to approximate those temperatures produced during fabrication and operation of a device [2, 13-14, 19]. The furnace was pre-set to the annealing temperature and allowed to stabilize for 1 hour before the specimens were inserted.

After stabilization, the specimens were put on a quartz boat and inserted into the front end of the tube. Following 10 minutes of preheating at this place, the specimens were inserted into the hot zone with a stainless steel rod and left in there for 1 hour. After the annealing period, the specimens were pulled out to the tube entrance and a cool-down period of 10 minutes was used prior to removal from the furnace. The samples were then removed and placed in dessicators while waiting for analysis.

In order to study the time dependence of the growth kinetics of hole formation in Au/Cu composite films at 400 ^{o}C, four samples were prepared from the same substrate and put into the tube furnace. Each one was taken out after annealing for the scheduled times (i.e., 450, 900, 1800, and 3600 sec) from the furnace.

3 3 Film characterization

3 3 1 Scanning Electron Microscopy

Following heat treatment, the topography of the outside film surface was characterized in a routine fashion at 25 KV or 30 KV using a scanning electron microscope with capabilities for EDS and B E image For the cross sectional view of the films, the specimens were mechanically fractured and coated with Au-Pd for analysis

3 3 2 Transmission Electron Microscopy

The internal grain structure of the films was examined in a transmission electron microscope For the preparation of specimens for transmission electron microscopy the films were removed from the quartz substrate by dissolving the quartz in 49% concentrated hydrofluoric acid and rinsing in de-ionized water before examination The grain size and the grain size distributions were measured by a line intercept method. The diffraction patterns were obtained by SAD in TEM and identified by measuring the distance of the diffraction rings from the center (transmitted beam) and using the formula [93] $R \times d = \lambda \times L$ where R is the distance of the diffraction pattern d is the interplanar spacing of a phase, λ is the wave length of the electron, and L is the camera constant of the microscope.

3.3 3 Auger Electron Spectroscopy

The chemical composition of the film surface was characterized using Auger electron spectroscopy (AES) The AES spectra were taken in the pulse counting N(E) mode and then differentiated using data processing computer incorporated in the Perkin Elmer PHI 660 Scanning Auger Multiprobe

Line scanning Auger microprobe (LSAM) was used to examine the lateral distribution of chemistry across the film surface.

A multiple-point Auger analysis was used to examine the difference of the chemical composition between a specific area and the matrix of the film. A 10 KeV electron beam with a probe diameter of about 0.1 μm was used for both the line scanning and the multiple-point Auger analysis.

Auger sputter profiling was used to examine the atomic species contained throughout the thickness of the films. Depth-composition profiles were made by argon sputtering with computer control alternating and data taking cycles. The critical conditions for the analysis were as follows: electron gun beam voltage: 10 KV, electron gun beam current: 0.01 μA, electron multiplier voltage: 1600 V, base pressure: $<1 \times 10^{-9}$ Torr (1.3×10^{-7} Pa), Pressure, Ar ion sputtering: 3×10^{-8} Torr (1.5×10^{-7} Pa), ion gun voltage: 3 KV, ion gun emission current: 25 mA, raster size: 3 x 3 (mm^2). Auger transitions of Cu LMM, Sn MNN, V LMM, Ti LMM, O KLL and Au NVV (or Au MNN for Au/Cu composite films) were used for the measurement of the peak-to-peak amplitude. The atomic concentrations (%) were calculated using data processing computer system incorporated in the Perkin-Elmer PHI 660 Scanning Auger Multiprobe and plotted as a graph illustrating the percentage of a particular element to the other elements as a function of sputter time.

$Cx = \{ (I_x/S_xT_xN_x(V/S)_x) / (\Sigma I_x/ S_xT_xN_x(V/S)_x) \} \times 100$

where: C = atomic concentration (%); I = peak-to-peak amplitude of the differentiated N(E) data, S = sensitivity factor; T = acquisition time per data point; N = number of sweeps; V/S = volts per steps. The relative Auger sensitivities used were as follows [94] Cu LMM = 200; Sn MNN = 530 V LMM = 208 Ti LMM = 168; O KLL = 350; Au NVV = .210; Au MNN = 053

3.3.4 X-ray Photoelectron Spectroscopy

The chemical states of metal oxides formed during isothermal annealing were characterized by XPS (Kratos-XSAM 800) The XPS data were obtained using Mg Kα radiation and operating the hemispherical analyzer at the medium resolution with a fixed retarding ratio (F R R) scan mode, in which the area of sample analyzed remains constant throughout the whole kinetic energy range. The position of C1s peaks were measured and moved at 284.6 eV [95]

3.3.5 X-ray Diffraction

For the texture of the films, X-ray diffraction patterns were obtained using CuK$_\alpha$ radiation (operated at 40 KV and 20 mA) and compared with the relative X ray Intensities I_{hkl}/I_{111}, of the randomly oriented gold powders which are listed in JCPDS (Jointed Committee of Powder Diffraction Standard)

CHAPTER 4
RESULTS AND DISCUSSION

4.1 Au/Cu Composite Films

4.1.1 Formation of Holes in Gold Films During Annealing

4.1.1.1 Surface Topography

Figure 6 shows typical SEM micrographs of Au/Cu composite films as-deposited and annealed at 300 °C, 400 °C and 500 °C for 1 hour in air, respectively. One observes the formation of holes in gold during annealing which appear as the darker regions. These dark circular spots were found to vary between 0.2 and 1.5 μm in diameter when the Au/Cu composite films annealed at 500 °C (Figure 7). The as-deposited Au/Cu composite films show little surface structure as can be seen in Figure 6a. This suggests that the as-deposited Au/Cu composite films have a very smooth surface. The surface smoothness of deposited films is determined by the statistical process of nucleation and growth, and the mobility of adatoms on the substrate surface [96]. The adatom mobility generally increases with increasing substrate smoothness. Thus, the smooth surface of the as-deposited Au/Cu composite films is believed to result from the smooth surface of substrate and that of the copper underlays deposited on it.

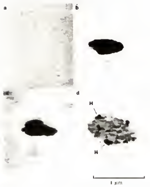

Figure 6 Scanning electron micrographs of as deposited and annealed Au/Cu composite films (60° tilt) (a) as deposited (b) 300 °C, (c) 400 °C and (d) 500 °C

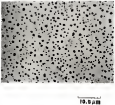

Figure 7 Scanning electron micrograph of a Au/Cu composite film annealed at 500 °C

Some of particular interest is Figure 6d in which a large gray area is observed which is dotted by black spots (marked "H"). It is believed that the large gray area stems from copper oxide (CuO) which is partially filling the hole in the gold film. Evidence for this will be given below.

4.1.1.2. Lateral Distribution of Chemistry Near the Holes

In order to study the nature of the holes shown in Figure 6, the regions of the dark spots were examined. Figure 8 depicts EDS data in SEM taken by focusing the beam on a dark spot and alternately onto the matrix of an annealed Au/Cu composite film. It can be seen that the ratio of Cu to Au signal is about 4.7 times larger on a dark spot compared to on the matrix. This suggests the depletion of gold in a dark spot. Both the information depth and the lateral resolution of EDS in SEM are about 1 µm [97]. The Si peaks in Figure 8a and 8b stem from the quartz substrate supporting the film. It is quite possible, considering the size of a dark spot and that of the probing beam, that the Au peak in Figure 8a (on a dark spot) may come from the surrounding gold matrix.

Figure 9 shows the Auger signal intensities for a line scan across a dark spot on the film surface of an annealed Au/Cu composite film. It is observed that the intensities of the copper and the oxygen signal decreases on a dark spot, while no gold signal intensity is detected across the film surface. Auger electron spectroscopy (AES) is the most widespread technique for studies of surface composition. In AES one uses Auger electrons with kinetic energies in the range of typically 10 to 2000 eV, with the corresponding inelastic mean free path (the escape depth of the electrons) on the order of 4 to 25 Å [98-99]. The probe diameter of scanning Auger microprobe was about 0.1 µm for the line scan using a

10-keV electron beam [100] Taking into account these analytical features it is suggested that the failure to observe a substantial Au signal on neither the matrix nor the dark spot is due to the presence of copper oxide both on the free surface of the gold film as well as in the holes. It will be shown in Section 4.1.2 that the kind of oxide which is formed this way is CuO rather than Cu_2O

The decreased Auger intensities of copper and oxygen on a dark spot in Figure 9b can be explained by considering "backscattering effects" on the Auger signal intensities Figure 10 shows a comparison of the secondary electron and the backscattered electron image of a dark spot in an annealed Au/Cu composite film. The dark spot in SEM appears as a darker region in the backscattered electron image The yield of backscattered electrons increases monotonically with the atomic number of the specimen as shown in Figure 11 [101] Specifically, the backscattered electron coefficient of gold is about 1.7 times larger than that of copper Thus a possible depletion of gold on a dark spot would generate less backscattered electrons than on the matrix, which result in the decreased Auger intensities of copper and oxygen on a dark spot in Figure 9b. This is consistent with the results of EDS analysis in Figure 8

An atomic multiple point Auger analysis was performed both on a dark spot and on the matrix of an annealed Au/Cu composite film with the resulting Auger spectra shown in Figure 12 The films were progressively sputtered for certain times and the Auger spectra were recorded at the same location after each sputtering interval The elements Cu O and C were evident both on a dark spot and on the matrix before sputtering (Figure 12, a1 and a2) C peaks are usually found on any samples which have been exposed to the atmosphere for any length of time

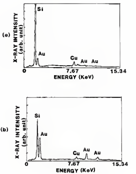

Figure 8 Energy dispersive spectroscopy (EDS) analysis of a Au/Cu composite film annealed at 500 °C (a) on a dark spot (b) on the matrix (in SEM)

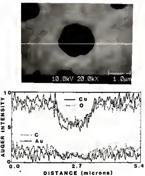

Figure 9 (a) Scanning electron micrograph of a Au/Cu composite film annealed at 500 °C
(b) Auger signal intensities for a line scan across the surface indicated in (a)

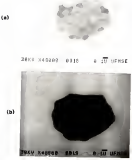

Figure 10 (a) Secondary electron and
(b) backscattered electron image
of a Au/Cu composite film annealed at 500 °C
(E_0=30 KeV).

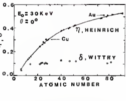

Figure 11. Comparison of secondary electron coefficient (δ) and backscattered electron coefficients (η) as a function of atomic number (Wittry, 1966, Heinrich, 1966) [from ref 101]

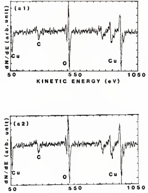

Figure 12. AES spectra taken from a Au/Cu composite film annealed at 500 °C
(a1) on a dark spot, (a2) on the matrix before sputtering
(b1) on a dark spot, (a2) on the matrix after 15 min sputtering
(c1) on a dark spot (c2) on the matrix after 45 min sputtering

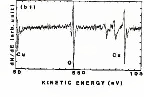

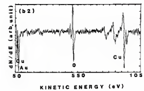

Figure 12 (continued)

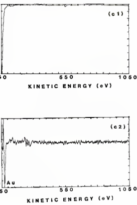

Figure 12. (continued)

before analysis [102-105] After 1.5 min sputtering however strong Au signal intensities were observed on the matrix along with Cu and O, while a dark spot was mostly Cu and O with no Au present (Figure 12, b1 and b2) The Auger analysis after 4.5 min sputtering indicates only a strong Au signal on the matrix, but a charging effect on a dark spot due to the exposure of quartz substrate (Figure 12, c1 and c2)

Figure 13 shows SEM and TEM micrographs of stripped Au/Cu composite films annealed at 500 °C after dissolving the quartz in 49 % HF solution Since the CuO layer was also dissolved in 49 % HF the former can not be seen in SEM nor in TEM micrographs as expected The dark region in an SEM micrograph and the white region in a TEM micrograph represents the holes in the gold films formed during annealing An Auger line scan (Figure 14b) for Au, Cu and O was taken along the line indicated on the SEM micrograph (Figure 14a) of a stripped Au/Cu composite film annealed at 500 °C Only a strong Au signal was observed on the matrix, while no Au, Cu or O were present in the hole of gold films This again suggests that Au/Cu composite films form holes during annealing in air Close correlation between the line scans and SEM images is evident

Furthermore, it is observed in Figure 13a that the gold is evenly distributed around the holes This suggests that the diffusion of gold atoms occurred during the formation of the holes resulting in an increase of overall film thickness

Figure 15 shows a fracture cross sectional SEM micrograph of an Au/Cu composite film annealed at 500 °C for 1 hour in air One observes the holes in the gold film which is partially filled with copper oxide (CuO)

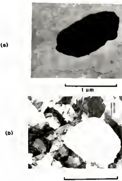

Figure 13 (a) Scanning electron micrograph and
(b) transmission electron micrograph of stripped Au/Cu composite films annealed at 500 °C (The films were removed from the substrate by dissolving the quartz in 49 % HF).

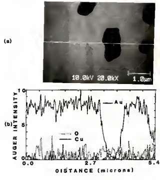

Figure 14 (a) Scanning electron micrograph of a Au/Cu composite film annealed at 500 °C
(b) Auger signal intensities for a line scan across the surface indicated in (a)

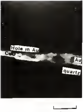

Figure 15 Fracture cross sectional SEM of an Au/Cu composite film annealed at 500 °C for 1 hour in air

Taking into account all the experimental evidence presented above we can now discuss certain models for the hole structure Figure 16 shows schematically a hole in an annealed Au/Cu composite film which is partially filled with copper oxide (CuO) To begin with we assume that copper oxide (CuO) forms on top of the gold matrix and also partially in the hole of the gold film as shown in Figure 16c As an alternative one can picture the hole in a gold film to be completely filled with copper oxide (Figure 16a) This possibility, however is discarded because of the observed charging effects on a dark spot (Figure 12 c1) after 4.5 min sputtering, while the gold matrix still showed a strong Au signal (Figure 12 c2) It could be argued that the sputtering yield for CuO is larger than that for Au Just the opposite, however is the case This will be explained in detail The ejection of atoms from the surface of a material by bombardment with energetic particles is called "sputtering" and the average number of atoms ejected from the material per incident ion is defined as the sputtering yield [106] The sputtering yield on gold has been reported to be higher than that of copper oxide [103 104] Thus the sputtering time before the exposure of the quartz substrate is expected to be longer on a dark spot than on the matrix In case of model A

Both, models B and C could satisfy the earlier presence of charging effects on a dark spot compared to on the gold matrix However the possibility of model B is discarded by the fracture cross sectional SEM of an annealed Au/Cu composite film at 500 °C (Figure 15)

Figure 17 shows a scanning electron micrograph of an annealed Au/Cu composite film which was obtained without tilting the specimen It is seen that the holes in the gold films which are partially filled with copper oxide exhibit

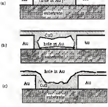

Figure 16 Schematic model structures of a hole in an annealed Au/Cu composite films which is partially filled with CuO
(a) Model A (b) Model B (c) Model C

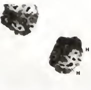

Figure 17 Scanning electron micrograph of an Au/Cu composite film annealed at 500 °C.

occasionally small holes marked "H" A large secondary electron signal around the edge compared to locations in the interior of the structure results in a white circular contrast around the holes in the CuO layer

It is concluded from these experiments that (1) Au/Cu composite films develop holes during annealing for 1 hour in air at temperatures between 300 °C and 500 °C, (2) The holes in the Au/Cu composite films are partially filled with copper oxide, (3) During the formation of the holes some gold atoms diffuse transversely resulting in an increase of overall film thickness

4 1 2 Formation of Copper Oxide During Annealing

Figure 18a shows the AES spectra taken from the Cu underlay in an as-deposited Au/Cu composite film in which the Au has been removed by 6 0 min argon sputtering. Figure 18b presents an AES spectra taken from the copper oxide layer near the film surface for an annealed Au/Cu composite film after 1 5 min sputtering It is evident that the copper underlay in an as-deposited Au/Cu composite film shows only a strong Cu signal with no O present, while the layer near the surface of an annealed Au/Cu composite film shows strong O and Cu signals Thus the chemical state of the copper underlay in an as-deposited Au/Cu composite film is metallic copper, which forms copper oxide during annealing in air and not during deposition

In order to identify the chemical state of the copper oxide, an XPS analysis was performed on an annealed Au/Cu composite film Figure 19 shows the characteristic CuO features in the XPS spectra Binding energies for the Cu $2P_{1/2}$ and $2P_{3/2}$ peaks are located at 953 8 eV and 933 8 eV, respectively These binding energies, the energy seperation of 20 0 eV between the two Cu 2P peaks and the

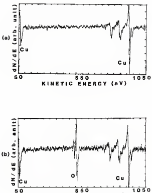

Figure 18 AES spectra taken from Au/Cu composite films
(a) as deposited (after 6.0 min. sputtering)
(b) annealed at 500 °C (after 1.5 min sputtering)

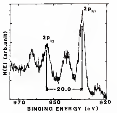

Figure 19 XPS spectra of the Cu 2p peaks taken from the surface of a Au/Cu composite film annealed at 500 °C.

"shake-up" peak at about 943 eV correspond to those of CuO [107]. Auger parameter (Cu LMM = 918 eV) plus photon energy (Cu $2P_{3/2}$ = 933.8 eV) also supports the formation of CuO rather than Cu_2O. The information depth of XPS is about 10 – 30 Å because of the escape depth of the electrons [98].

Thermodynamically, one would expect that copper oxide would form during deposition at the base vacuum pressure of 5×10^{-8} Torr. It is shown in the Richardson's chart [20] (Figure 1) that copper will oxidize in an atmosphere in which the partial pressure of oxygen is larger than about 10^{-42} atmosphere at room temperature. However, oxidation of copper may not occur if the kinetics are too slow [14]. From the kinetic theory of gases a relationship between the flux of incident molecules striking the surface of unit area per second and the ambient pressure is given as [108]

$$F(\text{molecules/cm}^2\text{-sec}) = 3.52 \times 10^{22}\ P(\text{Torr})(MT)^{-1/2}$$

where M is the average molecular weight of the gaseous species and T is the temperature. Substituting $P = 5 \times 10^{-8}$ Torr and using the values M = 32 g/mol and T = 300 K, the molecular impingement rate is about 10^{13} molecules/cm^2 sec. Assuming the surface concentration of copper is about 10^{15} atoms/cm^2, then the surface may be covered with a monolayer of copper oxide after 100 seconds if all the incident oxygen molecules that collide with the copper stick to it. Thus it is believed that a low impingement rate of oxygen to the thin film surface keeps the copper underlays from being oxidized during deposition at the base vacuum pressure of 5×10^{-8} Torr. The sticking coefficient of oxygen, that is, the fraction of incident gas particles that are absorbed by the film surface is also generally low [74, 109].

CuO is thermodynamically possible to form during annealing at 500 °C in air. For the chemical reaction $Cu + 1/2\ O_2 = CuO$, the Gibbs free energy for formation ($\Delta G = \Delta H - T\Delta S$ where ΔH is the change in enthalpy (or heat of reaction) during the reaction at temperature T and ΔS is the change in entropy) can be calculated from thermodynamic data [110]. Assuming $\Delta H(T) = \Delta H^{0}(298)$ and $\Delta S(T) = \Delta S^{0}(298)$ and using the values $\Delta H^{0} = -37.74$ kcal•mol^{-1} and $\Delta S^{0} = -22.07 \times 10^{-3}$ kcal•K^{-1}•mol^{-1}, the standard free energy for the formation of CuO is given as

$$\Delta G(\text{kcal}) = -37.74 + 22.07 \times 10^{-3}\ T\ (^{0}\text{K})$$

Since $RT\ln P_{O_2}$ (atm.) = $2\Delta G$ [111], CuO will form at 500 °C in an air atmosphere containing $P_{O_2} \geq$ about 10^{-11} atm. The formation of CuO in the Au/Cu system during annealing in a temperature range of 250 °C to 750 °C has been reported [59]. The growth of the Cu_2O phase from copper by thermal aging at 150 °C in an air has also been reported [102-104].

The overall composition of copper in an Au/Cu composite films was about 8.3 wt.% in this study. Reference to the phase diagram [112] shows that the solubility of Cu in Au is unlimited. Three possible intermetallic phases such as $CuAu_3$, CuAu, and Cu_3Au have been reported to form in Cu Au thin film couples during heat treatment [58, 113]. However, no evidence for the formation of intermetallic phases was observed by x ray diffraction, and XPS analysis.

It is believed that the copper from the underlays simply diffuse through the gold and form copper oxide (CuO) on the free surface of the gold films during annealing in air. Similar results were observed by Lee et al. in an Au/In composite film during annealing in air [10]. It was also reported by Lloyd et al. that the formation of intermetallic compounds was effectively reduced by the presence of a thin oxide layer grown on an Au/Pb thin film couple [56].

It can be concluded that Au/Cu composite films form copper oxide (CuO) during annealing in air and not during deposition. CuO is thermodynamically possible to form during annealing in air at the temperatures used in this study.

4.1.3 Distribution of Copper Throughout the Film

Auger depth-composition profiles were made applying argon ion sputtering with computer controlled alternating sputtering and data taking cycles. The resulting profiles are presented in terms of atomic concentration versus sputter etching time in Figure 20. As expected, copper is localized near the interface between the gold film and the quartz substrate in an as-deposited Au/Cu composite film (Figure 20a). High concentrations of copper and oxygen on the film surface are, however, observed for all chosen annealing temperatures (Figures 20b, 20c, and 20d). The oxidation might be the driving force for the out diffusion of the copper during annealing in air. However, surface segregation, concentration gradients, or strain effects during annealing could be also possible driving forces.

4.1.4 Grain Structure of Gold

Figure 21 depicts the grain structure of as deposited and annealed Au/Cu composite films as examined by TEM. The as-deposited Au/Cu composite films reveal a uniform and fine-grained structure with a mean grain diameter of about 700 Å (Figure 21a). The Au/Cu composite films develop substantial grain growth and holes in the gold films during annealing at 300 °C, 400 °C, and 500 °C (Figures 21b, 21c, and 21d, respectively). The mean grain diameter of annealed Au/Cu

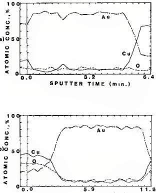

Figure 20 Auger sputter profiles of as-deposited and annealed Au/Cu composite films
(a) as-deposited (b) 300 °C
(c) 400 °C (d) 500 °C

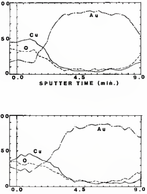

Figure 20 (continued)

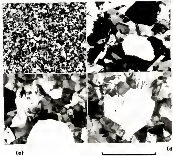

Figure 21: Transmission electron micrographs of as-deposited and annealed Au/Cu composite films (a) as-deposited, (b) 300 °C, (c) 400 °C and (d) 500 °C

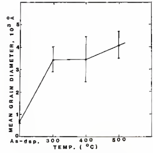

Figure 22. Mean grain diameters measured from transmission electron micrographs of as deposited and annealed Au/Cu composite films at various tempratures

composite films at 500 °C is about 4000 Å. The change in the mean grain diameter as a function of temperature is shown in Figure 22.

4.1.5 Fiber Texture (Preferred Orientation) of Gold

X-ray diffraction patterns of as-deposited and annealed Au/Cu composite films at 500 °C are shown in Figure 23a and 23b, respectively. Figure 23c shows the relative X-ray intensities, I_{hkl}/I_{111}, of the randomly oriented gold powders which are listed in JCPDS (Jointed Committee of Powder Diffraction Standard). Both as-deposited and annealed Au/Cu composite films reveal a strong {111} peak. X-ray diffraction occurs from the crystal planes which lie parallel to the substrate [114-115]. Thus, it is suggested that the gold films in as-deposited Au/Cu composite films have a (111) preferred orientation parallel to the substrate surface. The (111) preferred orientation of gold is retained after annealing up to 500 °C regardless of the annealing temperature.

It is well known that vapor deposited thin films tend to develop a preferred orientation, called "fiber texture" [116]. A fiber texture in vapor deposited thin films may develop at various stages, e.g., nucleation, coalescence, growth, epitaxial growth, oblique growth, and annealing. They are accordingly called nucleation, nucleation-growth, growth, epitaxial, oblique, and annealing texture, respectively [116]. The substrate, fused quartz, used in this study was amorphous and the films were deposited at about normal incidence on it. Thus the preferred orientation of gold in an as-deposited Au/Cu composite film is believed to develop at the stage of nucleation and growth during deposition.

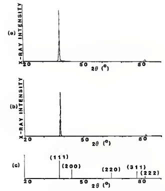

Figure 23 X-ray diffraction patterns of Au/Cu composite films.
(a) as-deposited
(b) annealed at 500 °C
(c) relative X-ray intensities I_{hkl}/I_{111}, of
Au powders listed in JCPDS

It is also generally agreed that vapor deposited films of fcc metals on amorphous substrates exhibit a (111) preferred orientation [116]. The (111) orientation of gold has been reported to have the lowest interfacial energy, and a higher nucleation rate than others [117-118]. The (111) preferred orientation in vapor deposited gold films on amorphous substrates has been observed before by other investigators [119-120].

4.1.6 Kinetic Study on the Formation of Holes in Au/Cu composite films

The number density, Na, of pores was counted using a grid of 3 x 4 μm^2 in size. The number of grid-crosses covered by holes out of 100 total grid-crosses, Pp, was also counted, and the area fraction, Aa, was then calculated by Aa = Pp/100. Relatively dense regions of holes were selected in the scanning electron microscope and the data were taken from ten different fields and averaged.

Figure 24 shows Na ($1/\mu^2$) and Aa (μ^2/μ^2) of holes in an annealed Au/Cu composite film for various annealing times. The scatter bar represents 95% confidence intervals for the mean ($\mu_x \pm 2$ S.E.) in both Figure 24a and 24b. Although the scatter was too large to draw a curve through the data with 95% confidence for the mean, it can be seen that the number of holes stays approximately equal with an annealing time, and the area fraction of holes increases with annealing time in near parabolic manner. This may suggest that the holes in the gold film form by a nucleation process and a diffusion rate control growth.

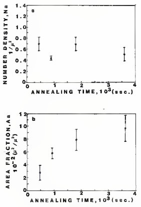

Figure 24 (a) Number density Na ($1/\mu m^2$) and (b) area fraction Aa ($\mu m^2/\mu m^2$) of holes of Au/Ca composite films annealed at 400 °C

Assuming the grain sizes are the same the number of triple points, N, per unit area is given as (private communication by R T DeHoff)

N = 2 x (1/area of a grain)

Taking 0.35 μm for the mean grain diameter (Figure 22) then the calculated number of grain boundary triple points per unit area (1/μm^{2}) is 20 for annealed Au/Cu composite films (400 ^{0}C, 1 hour) The number density of holes observed in Figure 24a is about 0.6 (1/μm^{2}) This is smaller than the calculated number of triple points Thus, it is suggested that even though the hole formation in gold films is likely to occur at the grain boundary triple points, there may be more favorable sites for hole formation than actually activated

It is concluded that (1) Au/Cu composite films form holes in the gold films during annealing for 1 hour in air at temperatures between 300 ^{0}C and 500 ^{0}C. The holes in Au/Cu composite films are partially filled with copper oxide (CuO), (2) Au/Cu composite films form copper oxide (CuO) during annealing in air and not during deposition (3) Cu underlays which have a small tendency towards oxidation do not prevent grain growth of gold during annealing. (4) The gold films in as-deposited Au/Cu composite films have a (111) preferred orientation parallel to the substrate. The (111) preferred orientation of gold is retained after annealing regardless of the annealing temperature (5) The density of holes in Au/Cu composite films stays nearly constant with annealing time, at 400 ^{0}C in air, while the area fraction of holes increases with annealing time in a near parabolic manner

4.2. Au/Sn Composite Films

4.2.1. Surface Topography

Figure 25 shows typical SEM micrographs of Au/Sn composite films as-deposited and annealed at 300 °C, 400 °C and 500 °C for 1 hour in air. It appears that annealing of the Au/Sn composite films at temperatures up to 500 °C does not substantially change the surface topography. Au/Sn composite films form neither hillocks nor holes during annealing in air. However, a rough surface structure in both, as-deposited and annealed composite films is observed in Figure 25. Figure 26 depicts an SEM micrograph of an as-deposited pure tin film of about 130 Å thickness. It exhibits similarly rough surface structure as that of an Au/Sn composite film. It is thus believed that the surface roughness of Au/Sn composite films results from the rough surface structure of the tin underlay. Similar results have been reported in Au/In composite films by Hummel et al. [3, 10]

4.2.2. Chemical State of Tin in As-deposited Au/Sn Composite Films

In order to study the change of the chemical state of tin throughout the film thickness, a series of AES spectra were taken using various sputtering times. The AES spectra were taken in the pulse counting N(E) mode and then differentiated using the data processing computer incorporated in the Perkin Elmer PHI 660 Scanning Auger Multiprobe. Figure 27 shows a series of Auger spectra taken from an as-deposited Au/Sn composite film. The top four AES spectra were taken from the surface region of the film, i.e., on the surface (Figure 27a), after 0.3 (Figure 27b), 0.9 (Figure 27c) and 1.5 (Figure 27d) min sputtering. The bottom three AES spectra were taken from the tin underlay region near the substrate, i.e., after 7.5 (Figure 27e), 8.1 (Figure 27f) and 8.7 (Figure 27g) min sputtering. The two major features

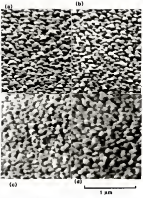

Figure 25 Scanning electron micrographs of as-deposited and annealed Au/Sn composite films (60° tilt) (a) as-deposited, (b) 300 °C, (c) 400 °C, and (d) 500 °C

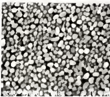

Figure 26 Scanning electron micrograph of an as-deposited pure tin film of 130 Å thickness

Figure 27 AES spectra, dN/dE, taken from an as-deposited Au/Sn composite film

I near surface
  (a) before sputtering
  (b) after 0.3 min. sputtering
  (c) after 0.9 min. sputtering
  (d) after 1.5 min. sputtering
II. near substrate
  (e) after 7.5 min. sputtering
  (f) after 8.1 min. sputtering
  (g) after 8.7 min. sputtering

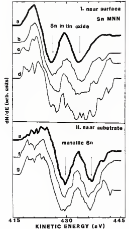
I. near surface
Sn MNN
Sn in tin oxide
a
b
c
d
dN/dE (arb. units)
II. near substrate
metallic Sn
e
f
g
415
430
445
KINETIC ENERGY (eV)

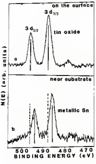

Figure 28 XPS spectra of the Sn 3d peaks taken from an as-deposited Au/Sn composite film
(a) on the surface
(b) near substrate

in Sn MNN peaks observed are known to be due to $M_4N_{4,5}N_{4,5}$ and $M_5N_{4,5}N_{4,5}$ Auger transitions [121,122]. The kinetic energies of the Sn MNN peaks at 430 and 437 eV correspond to those of metallic Sn [122-123]. This indicates that the chemical state of the tin underlay in as-deposited Au/Sn composite films remain in metallic form. In contrast to this, the kinetic energies of 425.5 and 433 eV near the film surface are consistent with those of tin oxide [122]. This indicates some out-diffusion and oxidation of Sn on the free surface of gold in an as-deposited Au/Sn composite film.

Similar changes of the chemical state of Sn throughout the film thickness were observed using XPS spectra performed on an as-deposited Au/Sn composite film. Figure 28 depicts a series of XPS spectra of the Sn 3d peaks taken on the surface (Figure 28a) and from the Sn underlay near the substrate after sputtering (Figure 28b). Figure 28a shows tin oxide features and Figure 28b shows metallic Sn features. Binding energies for the Sn $3d_{5/2}$ peak are located at 486.4 and 484.9 eV for tin oxide and metallic tin, respectively [124]. This is in agreement with the AES results (Figure 27).

In summary, the chemical state of the tin underlay in as-deposited Au/Sn composite films was found to be metallic tin. Some of the tin from the underlay diffuses out and forms tin oxide on the free surface of the gold films during storage at room temperature. Thermodynamically one would expect that tin would form tin oxide during deposition in vacuum of 5×10^{-8} Torr. It is shown in the Richardson's chart [20] (Figure 1) that tin will oxidize in an atmosphere in which the partial pressure of oxygen is larger than about 10^{-90} atmosphere at room temperature. However, as discussed in section 4.1.2, it is believed that a low impingement rate of oxygen to the film surface keeps tin underlays from being oxidized during deposition at the base vacuum pressure of 5×10^{-8} Torr

4.2.3 Formation of Tin Oxide During Annealing

A series of AES spectra were taken from an annealed Au/Sn composite film at 500 °C. As in the as-deposited Au/Sn composite film (Figure 27), the top four AES spectra were taken from the surface region of the film, i.e., on the surface (Figure 29a), after 0.3 (Figure 29b), 0.9 (Figure 29c) and 1.5 (Figure 29d) min sputtering. The bottom three AES spectra were taken from the tin underlay region near the substrate, i.e., after 7.5 (Figure 29e), 8.1 (Figure 29f) and 8.7 (Figure 29g) min sputtering. Kinetic energies (425.5 and 433 eV) throughout the film of an annealed Au/Sn composite film correspond to those of tin oxide [122].

Similar results were obtained by XPS analysis performed on annealed Au/Sn composite films at 300 °C. Figure 30 depicts a series of XPS spectra of the Sn 3d peaks taken on the surface (Figure 30a) and near the substrate (Figure 30b). All XPS spectra in Figures 30a and 30b show tin oxide features. The binding energy for the Sn $3d_{5/2}$ peak is located at approximately 486.4 eV. The slight difference of binding energies of the Sn 3d peaks on the surface of the film (Figure 30a) is believed to result from the surface contamination during air exposure before the analysis [122].

4.2.4 Identification of Oxide of Tin

Since it is difficult to distinguish the two stable oxides, namely SnO from SnO_2, by either AES or XPS because of their similar electronic structures [122], SAD patterns were used to identify the chemical state of tin oxide formed during annealing. Figure 31 shows a SAD pattern of an annealed Au/Sn composite film

Figure 29 AES spectra, dN/dE, taken from 500 °C annealed Au/Sn composite film

I. near surface
  (a) before sputtering
  (b) after 0.3 min sputtering
  (c) after 0.9 min sputtering
  (d) after 1.5 min sputtering
II. near substrate
  (e) after 7.5 min sputtering
  (f) after 8.1 min sputtering
  (g) after 8.7 min sputtering

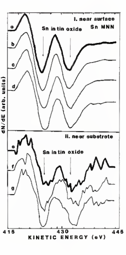
I. near surface
Sn MNN
Sn in tin oxide
a
b
c
d
dN/dE (arb. units)
II. near substrate
Sn in tin oxide
e
f
g
415
430
445
KINETIC ENERGY (eV)

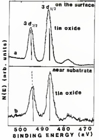

Figure 30 XPS spectra of the Sn 3d peaks taken from an annealed Au/Sn composite film at 500 °C
(a) on the surface
(b) near substrate.

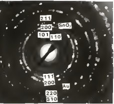

Figure 31 SnO_2 phase identified in an SAD pattern of an Au/Sn composite film annealed at 500 °C

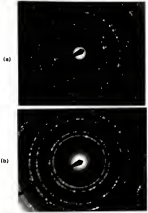

Figure 32 SAD patterns of Au/Sn composite films annealed at (a) 300 °C and (b) 400 °C.

The ring patterns of SAD in TEM suggest that both Au and SnO_2 are polycrystalline as expected. In addition to gold phases of (111), (200), (220) and (310), SnO_2 phases of (110), (101), (200) and (211) were observed as marked in Figure 31. Similar SAD patterns were also observed in Au/Sn composite films annealed at 300 °C and 400 °C as shown in Figures 32a and 32b, respectively.

In summary, it is suggested from these results that the tin underlay remains in a metallic form in an as-deposited Au/Sn composite film which oxidizes during annealing in air and forms tin oxide (SnO_2).

SnO_2 is thermodynamically possible to form during annealing in air. The Sn underlays could be oxidized during annealing by the following two mechanisms.

(1) mechanism A $Sn(liq.) + O_2 = SnO_2$ $(505\ ^{\circ}K \le T \le 1898\ ^{\circ}K)$

(2) mechanism B $Sn + O_2 = SnO_2$ $(298.16\ ^{\circ}K \le T \le 505\ ^{\circ}K)$

In mechanism A, the metallic tin is melted before it is oxidized and the liquid phase of tin then forms tin oxide (SnO_2) during annealing in air. In mechanism B, the metallic tin is oxidized before it is melted. For the chemical reaction, $Sn(liq.) + O_2 = SnO_2$, the Gibbs free energy of formation ($\Delta G = \Delta H - T\Delta S$) can be calculated from thermodynamic data [110]. Assuming $\Delta H(T) \approx \Delta H^{\circ}(298)$ and $\Delta S(T) \approx \Delta S^{\circ}(298)$ and using the values $\Delta H^{\circ} = -143.08$ kcal•mol^{-1} and $\Delta S^{\circ} = 52.153 \times 10^{-3}$ kcal•K^{-1}•mol^{-1}, the standard free energy for the formation of SnO_2 is given as

$$\Delta G(kcal) = -143.08 + 52.153 \times 10^{-3}\ T\ (^{\circ}K)$$

Since $RT\ln P_{O_2(atm)} = \Delta G$ [111], SnO_2 will form at $505\ ^{\circ}K \le T \le 773\ ^{\circ}K$ in an air atmosphere containing $P_{O_2} \ge$ about 10^{-30} atm.

For the chemical reaction, $Sn + O_2 = SnO_2$, the standard free energy for the formation of SnO_2 is given as

$\Delta G(\text{kcal}) = -142.01 + 48.803 \times 10^{-3}\, T\ (^{o}K)$

using the values $\Delta H^{o} = -142.01$ kcal•mol^{-1} and $\Delta S^{o} = -48.803 \times 10^{-3}$ kcal•K^{-1}•mol^{-1}. Again since $RT\ln P_{O_2(atm.)} = \Delta G$ [111], SnO_2 will form at 298.16 °K ≤ T ≤ 505 °K in atmosphere containing $P_{O_2} \geq$ about 10^{-52} atm. Thus SnO_2 is thermodynamically possible to form through both mechanism A and B during annealing in air.

The amount of tin in Au/Sn composite films was about 6.3 wt.% in this study. Reference to the phase diagram [125] shows that the solubility of Sn in Au at 500 °C is approximately 4.2 wt.%. There are three possible intermetallic phases such as AuSn, $AuSn_2$, and $AuSn_4$ which have been reported to form in Au/Sn system [54-56, 126-127]. Furthermore, Au has been reported to be a fast diffuser in Sn [128]. Thus interdiffusion might occur which might lead to these intermetallic phases. Also there might be the possibility of a Kirkendall effect with accompanying porosity [54-55]. However, no evidence for the formation of intermetallic phases was observed by SAD in TEM, X-ray diffraction, AES, and XPS.

It is thus concluded, as in Au/Cu composite films (Section 4.1.2.), that the tin from the underlay simply diffuses out and forms tin oxide (SnO_2) on the free surface of gold and along the grain boundaries of the gold films during annealing in air.

4.2.5 Distribution of Tin Throughout the Film

Auger depth-composition profiles were made by argon ion sputtering with computer controlled alternating sputtering and data taking cycles. The resulting profiles are presented in terms of atomic concentration versus sputter etching time in Figure 33. Figure 33a shows Auger depth profiles of an as-deposited Au/Sn composite film (30 days after deposition). Some of tin and oxygen can be observed

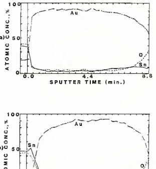

Figure 33 Auger sputter profiles of as-deposited and annealed Au/Sn composite films
(a) as deposited (30 days after deposition)
(b) 300 °C (c) 400 °C and (d) 500 °C

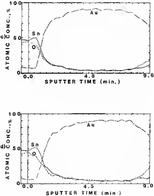

Figure 33 (continued)

already on the gold surface in this film. This may be interpreted by either (1) co-deposition of tin and gold, (2) the formation of an intermetallic compound by interdiffusion between gold and tin at room temperature or (3) out-diffusion of tin through gold grain boundaries either during evaporation or during storage at room temperature before analysis.

Firstly, if co-deposition of tin and gold had occurred, it would be expected that the concentration of tin would be uniformly throughout the entire gold film. This has not been observed. Therefore, this possibility is discarded.

Secondly, it has been reported that considerable interdiffusion can take place in as-deposited Au/Sn films resulting in the formation of various intermetallic phases such as AuSn, $AuSn_2$ and $AuSn_4$ at room temperature [54-56, 126-127]. Since Au is known to be a fast interstitial diffuser in Sn [128] but the Sn diffusivity in Au is negligibly small at room temperature [129], it is expected that any intermetallic compound would be formed whithin the region of the tin underlay. Furthermore, since gold was evaporated on top of tin and the overall composition of the film was about 6.3 wt. %Au, an unreacted pure gold layer is expected on the surface region even though all the tin might be consumed in forming the AuSn phase. It has been reported [126] that (1) if the concentration of tin in Au films is less than 50 atomic percent, the AuSn phase is then formed and grows from the interface leaving excess gold as an unreacted layer, (2) when the concentration of tin in Au is greater than 50 atomic percent, then the initially formed AuSn phase transforms subsequently into $AuSn_2$, and $AuSn_4$ or a mixture of both depending on the amount of excess tin. This possibility is however also discarded because (1) strong Auger intensities of tin and oxygen were observed on the film surface in Figure 33a, (2) the chemical state of tin underlays near the substrate was identified as metallic tin in an as-deposited Au/Sn composite films (Figure 27 and Figure 28), and (3) no evidence for the formation of intermetallic phases was observed by X-ray diffraction, AES, XPS and SAD in TEM.

Finally, the out-diffusion of tin is most likely to take place through the gold grain boundaries either during evaporation or during storage at room temperature before the analyses. It has been reported that the rapid diffusion of Sn into Au proceeds via grain boundaries [55]. The grain boundary diffusivity of Sn into Au at room temperature was reported to be $\geq 10^{-14}$ cm^2/sec [55]. The average diffusion distance after a time t is approximately given as $a \approx 2.4\sqrt{Dt}$ [130-131]. Substituting t = 30 days, then the diffusion distance of tin can be as much as about 3 µm during storage at room temperature which is more than film thickness.

The presence of oxygen may suggest the formation of tin oxide on the free surface of gold films which is in agreement with the results of AES (Figure 27) and XPS (Figure 28) analysis. Thus, the oxidation might be the driving force for the out diffusion of the tin even at room temperature. It is believed that the tin from the underlay diffused out through the gold films by grain boundary diffusion.

Compared to the as-deposited Au/Sn composite films, the thickness of the tin oxide layer on top of gold was increased during annealing as shown in Figures 33b, 33c and 33d. The apparent atomic concentration ratio of Sn to O is about 1 to 1.1 on the surface of annealed Au/Sn composite films. This seems to be contradictory to the results of SAD patterns in TEM in which SnO_2 was identified. The apparent difference is believed to be due primarily to the effect of backscattered electrons which might be produced by the gold matrix beneath the tin oxide layer. The backscattered energetic electrons change the intensity of the Anger signal which can be directly attributed to the incident electron beam [132] This may change the sensitivity factors of both tin and oxygen which is different from those used for the atomic concentration profiles in Figure 33 It is therefore believed that the results of SAD patterns in **TEM** in which SnO_2 was identified, are more reliable for the chemical state of tin oxide in this study

4 2 6 Grain structure of gold

Figure 34 depicts the grain structure of as deposited and annealed Au/Sn composite films as examined by TEM. Figure 35 shows the change in the mean grain diameter as a function of temperature. The scatter bar represents 95% confidence intervals for the mean ($\mu_x \pm 2$ S E) The identification of grain boundaries was difficult in the image of heavily faulted polycrystalline structures. This may introduce an error during the decision making process. Nonetheless, a slight grain growth during annealing is evident in Figure 34 Figure 36 shows a fracture cross-sectional scanning electron micrograph of an annealed Au/Sn composite films and exhibiting gold grains and a tin oxide (SnO_2) layer on top of the gold film

4 2 7 Fiber Texture (Preferred orientation) of gold

X-ray diffraction patterns of as-deposited and annealed Au/Sn composite films are shown in Figure 37. All major diffraction peaks of gold, i.e., the (111), (200), (220), (311), and (222) were observed both in as-deposited and in annealed Au/Sn composite films

In order to quantify a possible texture of thin films the orientational factor f_{hkl} is defined as [133]

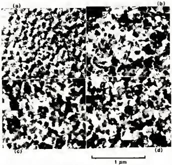

Figure 34 Transmission electron micrographs of as-deposited and annealed Au/Sn composite films (a) as-deposited (b) 300 °C, (c) 400 °C and (d) 500 °C

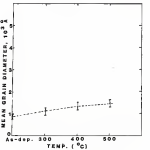

Figure 35 Mean grain diameters measured from transmission electron micrographs of as-deposited and annealed Au/Sn composite films at various temperatures

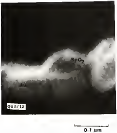

Figure 36. Fracture cross sectional scanning electron micrograph of an Au/Sn composite films annealed at 500 °C.

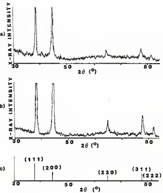

Figure 37 X-ray diffraction patterns of Au/Sn composite films
(a) as deposited
(b) annealed at 500 °C
(c) relative X-ray intensities, I_{hkl}/I_{111}, of Au powders listed in JCPDS

$f_{hkl} = (I_{hkl}/F_{hkl}) / \Sigma (I_{hkl}/F_{hkl})$,

where I_{hkl} and F_{hkl} are the measured intensity and the scattering factor for each diffraction plane (hkl), respectively. The values of the measured intensity and the scattering factor from the JCPDS are tabulated in Table 1. The resultant orientational factors calculated from the above equation are shown in Table 2. Considering all five major diffraction peaks in gold, the value $f_{hkl} = 0.20$ corresponds to samples having no preferred orientation. That is, the samples with $f_{hkl} = 0.20$ for all diffraction planes have randomly oriented structures.

It is suggested from these results that (1) the gold films in as-deposited Au/Sn composite films have a random orientation with a slightly stronger (200) orientation parallel to the substrate and (2) the random orientation of gold is essentially retained after annealing regardless of annealing temperature.

As discussed in section 4.1.5, it has been observed that evaporated gold films on an amorphous substrate exhibit a (111) preferred orientation [119-120]. Further, an increased mobility of aluminum atoms promotes the (111) preferred orientation of aluminum films [11]. It is believed that the decreased mobility of gold atoms arriving at the rough surface structure of the tin underlays, as shown in Figure 26, prevents the development of a (111) preferred orientation in gold films. This is similar to the Au/In system, where the rough surfaced indium underlays deposited onto an amorphous quartz substrate have been shown to cause a random orientation of gold both for as-deposited and for annealed polycrystalline films [10].

In summary, (1) Au/Sn composite films show a rough surface structure in both, as-deposited and annealed composite films. The surface roughness of Au/Sn composite films results from the rough surface structure of the Sn underlays, (2)

Table 1 Values of I_{hkl}/I_{111} and Scattering factor F_{hkl} of as-deposited and annealed Au/Sn composite films as measured by X ray diffraction

Diffraction Plane	Scattering Factor F_{hkl} (from JCPDS)	Au/Sn Composite Films I_{hkl}/I_{111} %			
		As dep.	300 °C	400 °C	500 °C
(111)	100	100	100	100	100
(200)	52	102	108	95	96
(220)	32	28	18	14	12
(311)	36	27	17	16	14
(222)	12	13	10	11	8

Table 2 Orientational factor f_{hkl} of as-deposited and annealed Au/Sn composite films as calculated from $f_{hkl} = (I_{hkl}/F_{hkl})/\Sigma(I_{hkl}/F_{hkl})$

Diffraction Plane	Au/Sn Composite Films Orientational Factor f_{hkl}			
	As-dep	300 °C	400 °C	500 °C
(111)	0.18	0.20	0.22	0.23
(200)	0.35	0.42	0.39	0.43
(220)	0.15	0.11	0.09	0.09
(311)	0.13	0.10	0.10	0.09
(222)	0.19	0.17	0.20	0.16

Au/Sn composite films form neither hillocks nor holes during annealing in air; (3) Au/Sn composite films form tin oxide (SnO_2) during annealing in air; (4) As deposited Au/Sn composite films form already a thin tin oxide layer on the free surface of gold without annealing, that is, during 30 days storage at room temperature The thickness of a tin oxide layer increases during annealing between 300 ºC and 500 ºC for 1 hour in air; (5) The gold films in as-deposited Au/Sn composite films have a random orientation with a slightly stronger (200) orientation parallel to the substrate surface The random orientation of gold is retained after annealing regardless of annealing temperature

4.3 Au/V Composite Films

4.3.1 Surface Topography

Figure 38 shows typical SEM micrographs of Au/V composite films as-deposited and annealed at 300 °C, 400 °C and 500 °C for 1 hour in air. As-deposited Au/V composite films reveal little surface structure as shown in Figure 38a. As discussed in Section 4.1.2.1, the smooth surface of an as-deposited films is believed to be due to the smooth surface of the substrate and that of the underlay. Hillock growth is apparent in annealed Au/V composite films (Figure 38b, 38c and 38d). The number density ($1/\mu m^2$) of the hillocks was about 13.5 ($1/\mu m^2$) (2 S.E = ± 2.2) and the area fraction of the hillocks was about 0.77 ($\mu m^2/\mu m^2$) (2 S.E = ± 0.04) in an annealed Au/V composite film (Figure 39). 2 S.E (standard error) represents 95% confidence intervals for the mean values.

In order to study the nature of the hillocks, atomic multiple-point Auger analysis was performed both on a hillock and on the matrix of an annealed Au/V composite film. Figure 40a and 40b shows Auger spectra taken on a hillock and on the matrix from an annealed Au/V composite film. The probe diameter of the scanning Auger microprobe was about 0.1 µm for the atomic multiple-point Auger analysis. It was difficult to direct the beam on either a hillock or on the matrix alone because of the highly compact hillocks of about 0.1 µm in width. This may cause Auger signals from the surrounding area during data aquisition. An image shifting by the electron beam made it even more difficult to use the line scanning Auger analysis across the film surface. Nonetheless, it is seen in Figure 40 that the ratio of the Au to the V signal was about 2.5 times larger on a hillock compared to on the matrix. This suggests that the hillocks consist mainly of Au.

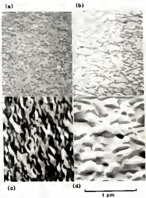

Figure 38 Scanning electron micrographs of as-deposited and annealed Au/V composite films (60° tilt)
(a) as-deposited (b) 300 °C
(c) 400 °C (d) 500 °C

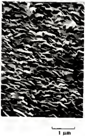

Figure 39 Scanning electron micrograph of an Au/V composite film annealed at 500 °C (60° tilt)

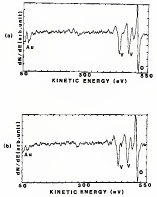

Figure 40 Auger spectra taken from an
Au/V composite film annealed at 500 °C
(a) on a hillock
(b) on the matrix

4.3.2 Formation of Vanadium Oxide During Annealing

In order to identify the chemical state of vanadium underlays in as-deposited Au/V composite films, AES spectra were taken after sputter etching. Figures 41a and 41b show Auger spectra taken from a vanadium underlay after 9.9 min and 10.5 min sputtering, respectively. The kinetic energies of the V LMM peaks at 431.5 and 437.5 eV have features of metallic vanadium [134].

Vanadium underlays form vanadium oxide during annealing in air. To investigate the chemical state of the vanadium oxide, an XPS analysis was performed on an annealed Au/V composite film. Figure 42 depicts XPS spectra of the V 2P peaks taken from the surface of a Au/V composite film annealed at 500 °C. Binding energies for the V $2P_{1/2}$ and $2P_{3/2}$ peaks were located at 524.9 eV and 517.4 eV, respectively. These binding energies and the energy seperation of 7.5 eV between the two V 2P peaks correspond to those of V_2O_5 [135]. The O 1s X-ray satellite is seen between the two V 2P peaks as marked in Figure 42. Figure 43 illustrates XPS spectra taken from the XPS handbook [135] of the V 2P peaks of the metallic V (Figure 43a) and those of V_2O_5 (Figure 43b). The differences in XPS spectra between metallic V and V_2O_5 are evident.

The information depth of XPS is about 10 - 30 Å caused by the escape depth of the electrons [98]. Thus the vanadium underlays cause vanadium oxide to form on the free surface of gold films during annealing in air. Its chemical state was identified as V_2O_5 in the XPS spectra.

Thermodynamically one would expect that vanadium would form vanadium oxide during deposition at the base vacuum pressure of 5 x 10^{-8} Torr. As shown in the Richardson's chart [20] (Figure1), vanadium oxidizes in an atmosphere in which

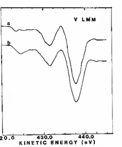

Figure 41 AES spectra taken from an as-deposited Au/V composite film:
(a) vanadium underlay after 9.9 min sputtering
(b) vanadium underlay after 10.5 min sputtering

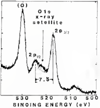

Figure 42 XPS spectra of the V 2p peaks taken from the surface of an Au/V composite film annealed at 500 °C

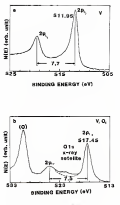

Figure 43 XPS spectra of (a) metallic V and (b) V_2O_5 [from ref. 135]

the partial pressure of oxygen is larger than about 10^{-100} atmosphere at room temperature. Thus vanadium is very likely to be oxidized at a very low partial pressure of oxygen. However, as discussed in Section 4.1.2, it is believed that a low impingement rate of oxygen keeps vanadium underlays from being oxidized during deposition at the base vacuum pressure of 5×10^{-8} Torr.

V_2O_5 is thermodynamically possible to form during annealing at 500 °C in air. For the chemical reaction $2V + 5/2\ O_2 = V_2O_5$ the Gibbs free energy for the formation ($\Delta G = \Delta H - T\,\Delta S$) can be calculated from thermodynamic data [110]. Assuming $\Delta H(T) = \Delta H^o(298)$ and $\Delta S(T) = \Delta S^o(298)$ and using the values $\Delta H^o = -381.96$ kcal•mol^{-1} and $\Delta S^o = 177.39 \times 10^{-3}$ kcal•K^{-1}•mol^{-1}, the standard free energy for the formation of V_2O_5 is given as

$$\Delta G\ (\text{kcal}) = -381.96 - 176.39 \times 10^{-3}\ T\ (^oK)$$

Since $RT\ln P_{O_2(atm)} = 2/5\ \Delta G$ [111], V_2O_5 will form at 500 °C in an air atmosphere containing $P_{O_2} \geq$ about 10^{-59} atm.

In order to study the change of the chemical state of vanadium throughout the film thickness, a series of AES spectra were taken at various sputtering times. The AES spectra were taken in the pulse counting N(E) mode and then differentiated using the data processing computer incorporated in the Perkin-Elmer PHI 660 Scanning Auger Multiprobe. Figure 44 shows a series of Auger spectra taken from an annealed Au/V composite film. The top four AES spectra were taken from the surface region of the film, i.e., on the surface (Figure 44a), after 0.3 (Figure 44b), 0.9 (Figure 44c) and 1.5 (Figure 44d) min sputtering. The bottom three AES spectra were taken from the vanadium underlay region near the substrate, i.e., after 18.5 (Figure 44e), 17.5 (Figure 44f) and 17.7 (Figure 44g) min sputtering.

It is seen in Figure 44 that the kinetic energy of the V LMM peaks appears at about 436 eV throughout the film of the annealed Au/V composite film. As mentioned above, the chemical state of vanadium oxide formed during annealing in air is V_2O_5. Thus the Auger spectra in Figure 44 are believed to be due to the formation of vanadium oxide (V_2O_5) throughout the film.

The chemical reactions of vanadium with the SiO_2 substrate during annealing have been widely discussed in the literature. It has been reported that the most reactive of the transition metals (e.g. titanium, zirconium, hafnium, vanadium, niobium) can be expected to adhere to SiO_2 quite well [17, 136-137]. The reason for the excellent adhesion to SiO_2 is that they have a negative heat of reaction with SiO_2 which breaks down SiO_2 to form oxides of the transition metals during a heat treatment in which external oxygen sources are absent (e.g. high vacuum) [17, 136].

Assuming that the reaction products are a metal silicide and a metal oxide, the chemical reaction can be given as [136]

$$SiO_2 + M_x = M_ySi + M_{x-y}O_2$$

where M is the metal.

The change in the Gibbs free energy, ΔG, is given by [138]

$$\Delta G = \Delta H - T\Delta S$$

where ΔH is the change in enthalpy (or heat of reation) during the reaction at temperature T, and ΔS is the change in entropy. If ΔG is less than zero, the reaction is thermodynamically possible. For the reactions in the solid state, ΔS = 0, because the volume changes are negligibly small [136]. Thus the change in Gibbs free energy ΔG is approximated by the change in enthalpy ΔH.

Figure 44. AES spectra dN/dE taken from an Au/V composite film annealed at 500 °C

I. near surface
  (a) before sputtering
  (b) after 0.3 min. sputtering
  (c) after 0.9 min. sputtering
  (d) after 1.5 min. sputtering
II near substrate
  (e) after 16.5 min. sputtering
  (f) after 17.1 min. sputtering
  (g) after 17.7 min. sputtering

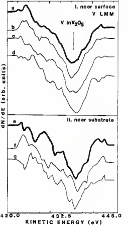
I. near surface
V LMM
V in V_2O_5
a
b
c
d
II. near substrate
e
f
g
dN/dE (arb. units)
420.0
432.5
445.0
KINETIC ENERGY (eV)

In the case of vanadium, it has been reported that vanadium forms V_3Si with the SiO_2 substrate during annealing under vacuum at about 800 °C for 3 hour [136]. The vanadium silicide forms towards the substrate side of the metal film, while the metal oxide forms on the free surface [136].

In this study, it was difficult to get Auger informations after exposure of the quartz substrate because of charging effects. It is thus not demonstrated whether the vanadium underlays reacted and formed vanadium silicides with the SiO_2 substrate during annealing at 500 °C in air.

The concentration of vanadium in Au/V composite films was about 5.5 wt % in this study. Reference to the phase diagram [139] shows that the solubility of V in Au at 500 °C is approximately 4.0 wt %. It is, however, believed by considering the results of XPS in Figure 42 and the results of AES in Figure 44 that vanadium underlay mainly form vanadium oxide (V_2O_5) during annealing in air.

4.3.3 Distribution of Vanadium Throughout the Film

Auger depth profiles were made by argon ion sputtering with computer controlled alternating sputtering and data taking cycles. The resulting profiles are presented in terms of atomic concentration versus sputter etching time in Figure 45. Auger depth profiles of as-deposited and annealed Au/V composite films at various temperatures are seen. As expected, vanadium is localized near the interface between the gold film and the quartz substrate in an as-deposited Au/V composite film (Figure 45a). High concentrations of vanadium and oxygen on the film surface were, however, observed for all chosen annealing temperatures (Figures 45b, 45c, and 45d), which supports the concept of out-diffusion of the vanadium underlay and the formatino of a vanadium oxide (V_2O_5) on the free surface and in the grain boundaries of gold during annealing in air. Thus oxidation might be again a driving force for the out-diffusion of vanadium during annealing in air as discussed in Section 4.1.3.

4.3.4 Grain Structure of gold

Figure 46 depicts the grain structure of as-deposited and annealed Au/V composite films examined by TEM. The as-deposited Au/V composite films reveal a relatively uniform and fine-grained polycrystalline structure with a mean grain diameter of about 1000 Å (Figure 46a). The annealed Au/V composite films show grain growth in gold when annealed at 300 °C, 400 °C and 500 °C (Figures 46b, 46c and 46d, respectively). The mean grain diameter of annealed Au/V composite films at 500 °C was about 2700 Å. The change in the mean grain diameter as a function of temperature is shown in Figure 47.

4.3.5 Fiber Texture (Preferred Orientation) of Gold

X-ray diffraction patterns of as-deposited and annealed Au/V composite films are shown in Figure 48a and 48b, respectively. Figure 48c shows the relative X-ray intensities, I_{hkl}/I_{111} of the randomly oriented gold powders which is listed in JCPDS (Joint Committee of Powder Diffraction Standard). Both as-deposited and annealed Au/V composite films reveal a strong (111) peak in X-ray diffraction.

Similarly as discussed in section 4.1.5., it is suggested that gold films in as-deposited Au/V composite films have a (111) preferred orientation parallel to the substrate surface. The (111) preferred orientation of gold is retained after annealing regardless of the annealing temperatures up to 500 °C.

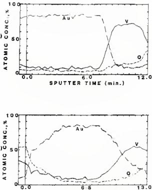

Figure 45 Anger sputter profiles of as-deposited and annealed Au/V composite films:
(a) as-deposited (b) 300 °C
(c) 400 °C (d)500 °C

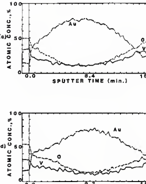

Figure 45 (continued)

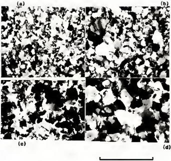

Figure 46 Transmission electron micrographs of as-deposited and annealed Au/V composite films (a) as-deposited (b) 300 °C (c) 400 °C and (d) 500 °C

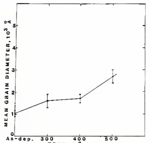

Figure 47 Mean grain diameters measured from transmission electron micrographs of as-deposited and annealed Au/V composite films at various temperatures

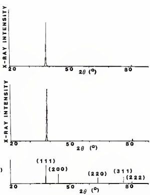

Figure 48 X ray diffraction patterns of Au/V composite films
(a) as-deposited
(b) annealed at 500 °C
(c) relative X ray intensities, I_{hkl}/I_{111}, of Au powders listed in JCPDS

In summary, (1) Au/V composite films form hillocks during annealing in air which mainly consist of Au; (2) V underlays sandwiched between gold thin films and substrate from vanadium oxides (V_2O_5) on the free surface of gold and along the grain boundaries of the gold films during annealing in air; (3) The gold films in Au/V composite films have a (111) preferred orientation parallel to the substrate surface. The (111) preferred orientation of gold is retained after annealing regardless of annealing temperature.

4.4 Au/Ti Composite Films

4.4.1 Formation of Gold Hillocks During Annealing

4.4.1.1 Surface Topography

Figure 49 shows typical SEM micrographs of Au/Ti composite films as deposited and annealed at 300 °C, 400 °C and 500 °C for 1 hour in air. The formation of hillocks are observed which developed during annealing. As-deposited Au/Ti composite films show little surface structure as shown in Figure 49a. As discussed in Section 4.1.1.1, the smooth surface of the as-deposited films is believed to be due to the smooth surface of the substrate and that of the titanium underlays deposited on it. Au/Ti composite films form hillocks during annealing at 400 °C and 500 °C (Figures 49c and 49d, respectively). In contrast to the hillocks in Au/V composite film (section 4.3), those in Au/Ti composite films extended on the surface of gold films and presented well defined geometrical faces probably corresponding to a (111) orientation of gold.

Figure 50a and 50b show lower magnification SEM micrographs of Au/Ti composite films annealed at 400 °C and 500 °C for 1 hour in air, respectively, exhibiting the distribution of hillocks on the surface of gold films. The size and density of hillocks do not seem to be much different between Au/Ti composite films annealed at 400 °C and 500 °C. The size of the hillocks was found to vary between about 0.1 and 1.0 μm in diameter in annealed Au/Ti composite films at 500 °C (Figure 50b). The number density ($1/\mu m^2$) of the hillocks was about 0.32 ($1/\mu m^2$) (2 S.E. = ±0.16) and the area fraction of the hillocks was about 0.06 ($\mu m^2/\mu m^2$) (2 S.E. =±0.01) (Figure 50b). Figure 51 shows hillocks formed on the surface of gold films examined by scanning electron microscopy for an annealed

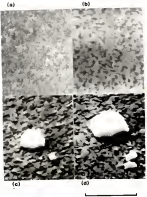

Figure 49 Scanning electron micrographs of as-deposited and annealed Au/Ti composite films (60° tilt)
(a) as deposited (b) 300 °C
(c) 400 °C (d) 500 °C

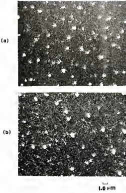

Figure 50 Scanning electron micrographs of annealed Au/Ti composite films
(a) 400 °C (b) 500 °C

Figure 51 Scanning electron micrograph of an Au/Ti composite film annealed at 500 °C (90° tilt)

Au/Ti composite films. The height of the hillocks was observed to vary between about 0.02 and 0.2 µm.

4.4.1.2. Lateral Distribution of Chemistry Near the Hillocks

In order to study the nature of the hillocks, the regions surrounding the hillocks were examined. Figure 52 shows the Auger signal intensities for a line scan across the film surface of an Au/Ti composite film annealed at 500 °C. The probe diameter of the scanning Auger microprobe was about 0.1 µm for the line scan. The hillock regions showed a pronounced increase in the gold signal while the titanium signal and the oxygen signal was diminished. This suggests that the hillocks in question consist mainly of gold.

Atomic multiple-point Auger analysis was performed both on a hillock and on the matrix of an Au/Ti composite film annealed at 500 °C with the resulting Auger spectra shown in Figure 53. The elements Ti, O, Au and C were evident both on the hillock and on the matrix (Figure 53a and 53b, respectively). It is, however, interesting to note that the Auger intensity ratio of Au to Ti was about 5.2 times larger on the hillock compared to in the matrix. This supports the result of the line scanning Auger analysis in Figure 52 that hillocks mainly consist of gold. It is not certain that the hillocks are composed of a two-phase alloy of Au and TiO_2 in the atomic multiple-point Auger analysis. C peaks are usually found on all samples which have been exposed to atmosphere for any length of time before analysis [102-105].

Figure 54a shows a TEM micrograph of a stripped Au/Ti composite film annealed at 500 °C by dissolving the quartz substrate in 49 % HF solution. The darker contrast of the hillocks in TEM is due to an increase in thickness of the film

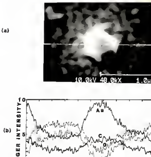

Figure 52. (a) Scanning electron micrograph of a Au/Ti composite film annealed at 500 °C
(b) Auger signal intensities for a line scan across the surface indicated in (a)

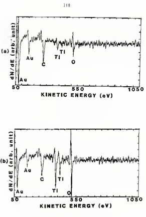

Figure 53. Auger spectra taken from an Au/Ti composite film annealed at 500 °C
(a) on a hillock
(b) on the matrix

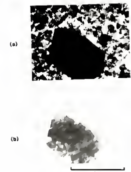

Figure 54 Transmission electron micrographs of hillocks formed in an Au/Ti composite film annealed at 500 °C. (The darker area is the hillocks)
(a) lateral growth of hillocks above the gold film
(b) over exposured to bring out the grain structure of gold films below the hillock in (a).

where the hillocks are situated. Figure 54b shows over exposured TEM micrograph to reveal the grain structure of the gold films below the hillock. It is seen that the grain structure of gold is also continued below the hillocks, i.e., the gold hillocks grow and laterally expand on top of the gold films. Thus, a hillock experiences both lateral expansion and growth of height on top of gold film during annealing.

4.4.2 Formation of Titanium Oxide During Annealing

In order to identify the chemical state of titanium underlays in an as-deposited Au/Ti composite films, AES spectra were taken after sputtering the gold films. The AES spectra were taken in the pulsed counting N(E) mode and then differentiated using the Perkin-Elmer 7000 Computer System incorporated in the Perkin-Elmer PHI 660 Scanning Auger Multiprobe. Figures 55a and 55b show Auger spectra taken from the titanium underlays after 6.9 min. and 7.5 min. sputtering, respectively. The kinetic energies of the Ti LMM peaks at about 382.5 and 387.5 eV are believed to be those of the metallic titanium. Compared to 383 and 388 eV for metallic Ti in Auger Hand Book [140], the 0.5 eV difference of kinetic energies for both peaks may result from charging effects. The Ti LMM peaks of TiO_2 appear as one single peak at about 383 eV [141]. The intensity ratio of Ti LMM/LMV transitions can be also used for the determination of chemical states [141].

The titanium underlays cause titanium oxide to form during annealing in air. In order to investigate the chemical state of titanium oxide, an XPS analysis was performed on annealed Au/Ti composite films. Figure 56 depicts the XPS spectrum of the Ti 2P peaks taken from the surface of a Au/Ti composite film annealed at 500 ^{0}C. Binding energies for the Ti $2P_{1/2}$ and $2P_{3/2}$peaks were located at 464.6 eV

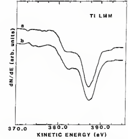

Figure 55 AES spectra taken from an as-deposited Au/Ti composite film
(a) Titanium underlay after 6.9 min. sputtering
(b) Titanium underlay after 7.5 min. sputtering

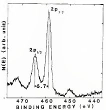

Figure 56 XPS spectra of the Ti 2p peaks taken from the surface of an Au/Ti composite film annealed at 500 °C

and 458.9 eV, respectively. These binding energies and the energy seperation of 5.7 eV between the two Ti 2P peaks correspond to those of TiO_2 [142]. The information depth of XPS is about 10 - 30 Å because of the escape depth of the electrons [98]. Thus titanium underlays cause titanium oxide (TiO_2) to form on top of gold films during annealing in air. The Au signal on the surface (Figure 53) suggests that titanium oxide (TiO_2) does not form a complete film on top of gold films. This is probably due to the Au hillocks formed on the surface of the gold films during annealing.

Thermodynamically, one would expect that titanium would oxidize during deposition at the base vacuum pressure of 5 x 10^{-8} Torr. It is shown in the Richardson's chart [20] (Figure 1) that titanium will oxidize in an atmosphere in which the partial pressure of oxygen is larger than about 10^{-150} atmosphere at room temperature. Thus titanium is very likely to be oxidized at a very low partial pressure of oxygen. However, a low sticking coefficient of oxygen to the film surface generally prevent the formation of oxide during deposition [74]. It has been found that there is a need for a very high ratio of oxygen to metal atoms in order to form TiO_2 [74, 143]. It is therefore believed that a low sticking coefficient of oxygen on the thin film surface keeps titanium from being oxidized during deposition at the base vacuum pressure of 5 x 10^{-8} Torr.

Thermodynamically, TiO_2 is likely to form during annealing at experimental temperatures used in this study. For the chemical reaction, $Ti + O_2 = TiO_2$, the standard free energy of formation ($\Delta G = \Delta H - T\,\Delta S$) can be calculated from the thermodynamic data [110]. Assuming $\Delta H(T) = \Delta H^0(298\ ^0K)$ and $\Delta S(T) \approx \Delta S^0(298\ ^0K)$

and using the values $\Delta H^{\circ} = -228.36$ kcal•mol^{-1} and $\Delta S^{\circ} = -44.33 \times 10^{-3}$ kcal•K^{-1}•mol^{-1}, the standard free energy for the formation of TiO_2 is given as

$$\Delta G\ (\text{kcal}) = -228.38 + 44.33 \times 10^{-3}\ T\ (^{\circ}K)$$

Since $RT\ln P_{O_2(\text{atm})} = \Delta G$ [111] TiO_2 will form at 500 °C in an air atmosphere containing $P_{O_2} \geq$ about 10^{-55} atm.

In order to study the change of the chemical state of titanium throughout the film thickness, a series of AES spectra were taken at various sputtering times. The AES spectra were taken in the pulse counting N(E) mode and then differentiated using the data processing computer incorporated in the Perkin-Elmer PHI 660 Scanning Auger Multiprobe. Figure 57 shows a series of Auger spectra taken from an annealed Au/Ti composite film. The top four AES spectra were taken from the surface region of the film, i.e. on the surface (Figure 57a) after 0.3 (Figure 57b), 0.9 (Figure 57c) and 1.5 (Figure 57d) min sputtering. The bottom three AES spectra were taken from the vanadium underlay region near the substrate, i.e., after 9.9 (Figure 57e), 10.5 (Figure 57f) and 11.1 (Figure 57g) min sputtering.

It is seen in Figure 56 (a-d) that the kinetic energies of the Ti LMM peaks appear at about 383 eV near the film surface of an Au/Ti composite film annealed at 500 °C. The chemical state of titanium oxide formed during annealing in air was identified as TiO_2 in XPS spectra [Figure 56]. Thus the Auger spectra near the film surface in Figure 57 (a-d) are believed to be those of titanium oxide (TiO_2) formed during annealing in air.

It is not clear whether the two peaks at about 381.5 and 386 eV in Figure 57 (e-g) reveal that titanium underlays react with SiO_2 and form titanium silicide and

Figure 57 AES spectra dN/dE taken from an Au/Ti composite film annealed at 500 °C

I near surface
  (a) before sputtering
  (b) after 0.3 min. sputtering
  (c) after 0.9 min sputtering
  (d) after 1.5 min sputtering
II. near substrate
  (e) after 9.9 min sputtering
  (f) after 10.5 min sputtering
  (g) after 11.1 min. sputtering

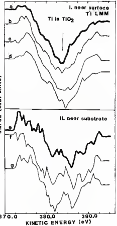
I. near surface
Ti LMM
Ti in TiO$_2$
a
b
c
d
II. near substrate
e
f
g
dN/dE (arb. units)
370.0
380.0
390.0
KINETIC ENERGY (eV)

titanium oxide during annealing at 500 ^{0}C in air because of the high noise level near the quartz substrate

Titanium has been reported to react with SiO_2 and to form titanium silicide and titanium oxide during annealing in cases in which external oxygen is absent (e g, high vacuum) [17, 136] This is, as discussed in Section 4.3.2., known due to the negative heat of reaction (ΔH) for this chemical reaction. Furthermore, it is noted in the Richardson's chart [20] that Ti has stronger tendency towards oxidation than Si (Figure 1). It is possible that Ti from the underlay might be reacted with the SiO_2 substrate during annealing even in air and form titanium silicide and titanium oxide

The overall composition of titanium in Au/ Ti composite films was about 3.7 wt.% Ti in this study. Reference to the phase diagram [144] shows that the solubility of Ti in Au at 500 ^{0}C is less than 1.0 wt.% It is however believed that titanium underlays mainly form titanium oxide (TiO_2) on the free surface of gold and along the grain boundaries of gold films during annealing in air

4.4.3 Distribution of Titanium Throughout the Film

Auger depth-composition profiles were made by argon ion sputtering with computer controlled alternating sputtering and data taking cycles The resulting profiles are presented in terms of atomic concentration versus sputter etching time (Figure 58) Auger depth profiles of as-deposited and annealed Au/Ti composite films at various temperatures are seen As expected, titanium is localized near the interface between the gold film and the quartz substrate in the as-deposited Au/Ti composite film (Figure 58a) High concentrations of titanium and oxygen on the film surface were, however, observed for all chosen annealing temperatures

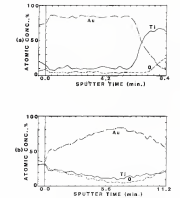

Figure 58 Auger sputter profiles of as-deposited and annealed Au/Ti composite films
(a) as-deposited (b) 300 °C
(c) 400 °C (d)500 °C

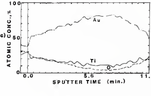

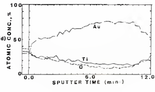

Figure 58 (continued)

[Figures 58b, 58c, and 58d], which supports the concept of out-diffusion of the titanium from the underlays and the formation of a titanium oxide (TiO_2) on the free surface of gold during annealing in air. Thus the oxidation might be the driving force for the out-diffusion of the titanium underlays during annealing in air as discussed in Section 4.1.3.

4.4.4 Grain Structure of Gold

Figure 59 depicts the grain structure of as-deposited and annealed Au/Ti composite films examined by TEM. The as-deposited Au/Ti composite films revealed an uniform and fine-grained polycrystalline structure with a mean grain diameter of about 1000 Å (Figure 59a). The annealed Au/Ti composite films showed little grain growth in gold when annealed at 300 ^{0}C, 400 ^{0}C, and 500 ^{0}C (Figures 59b, 59c, and 59d, respectively). The change in the mean grain diameter as a function of temperature is shown in Figure 60. It is apparent that Ti underlays which have a strong tendency towards oxidation prevent the grain growth of gold during annealing in air.

4.4.5 Fiber Texture (Preferred Orientation) of Gold

X-ray diffraction patterns of as-deposited and Au/Ti composite films annealed at 500 ^{0}C are shown in Figure 61a and 61b, respectively. Figure 61c shows the relative X-ray intensities, I_{hkl}/I_{111}, of the randomly oriented gold powders which are listed in JCPDS (Jointed Committee of Powder Diffraction Standard). Both as-deposited and annealed Au/Ti composite films revealed a strong (111) peak in X-ray diffractions.

As discussed in Section 4.1.5, it is suggested that the gold films in as-deposited Au/Ti composite films have a (111) preferred orientation parallel to the

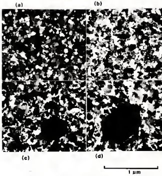

Figure 59 Transmission electron micrographs of as-deposited and annealed Au/Ti composite films (a) as-deposited (b) 300 °C, (c) 400 °C and (d) 500 °C

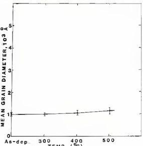

Figure 60 Mean grain diameters measured from transmission electron micrographs of as-deposited and annealed Au/Ti composite films at various temperatures

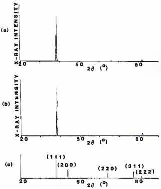

Figure 61 X-ray diffraction patterns of Au/Ti composite films
(a) as-deposited
(b) annealed at 500 °C
(c) relative X-ray intensities I_{hkl}/I_{111}, of
Au powders listed in JCPDS

substrate surface, and the (111) preferred orientation of gold is retained after annealing regardless of the annealing temperatures up to 500 °C.

It is concluded that (1) Au/Ti composite films form hillocks during annealing in air which mainly consist of Au; (2)Ti underlays sandwiched between gold thin films and substrate form oxides (TiO_2) on the free surface and along the grain boundaries of the gold films during annealing in air; (3) Ti underlays which have a strong tendency towards oxidation prevent grain growth of gold during annealing in air. This is interpreted to be caused by a capping of the gold surface and pinning the grain boundaries of the gold films by the oxide; (4) The gold films in as-deposited Au/Ti composite films have a (111) preferred orientation parallel to the substrate. The (111) prefered orientation of gold is retained after annealing regardless of the annealing temperature.

4.5 Summary

4.5.1 Oxides

Cu-, Sn-, V-, and Ti- underlays sandwiched between gold thin films and substrate form oxides (CuO, SnO_2, V_2O_5 and TiO_2 respectively) on the free surface of gold and in the grain boundary region of the gold films during annealing in air. Thermodynamically, one expects that all of these underlays will oxidize during deposition at the base vacuum pressure of 5x10^{-8} Torr. It is however, believed that these underlays in as-deposited gold composite films remain in metallic form because of a low sticking coefficient of oxygen to the thin film surface during deposition.

As-deposited Au/Sn composite films form a thin tin oxide layer on the free surface of gold without annealing, that is, during 30 days storage at room temperature. This is believed to result from grain boundary diffusion of tin through gold at room temperature.

4.5.2 Grain Growth

Figure 62 shows the changes in the mean grain diameters of as-deposited and annealed gold composite films as a function of temperature. It is seen that Ti underlays which have a strong tendency towards oxidation are most suited for the prevention of grain growth of gold during annealing in air, while Cu underlays which have a small tendency towards oxidation do not prevent grain growth of gold during annealing in air. The oxides which formed during annealing reduce in most cases the tendency towards growth of the gold grains. This is interpreted to be caused by a capping of the gold surface and by pinning the grain boundaries of the gold films by the oxide.

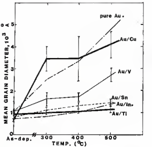

Figure 62 Mean grain diameters measured from transmission electron micrographs of as-deposited and annealed Au/Cu, Au/Sn Au/V and Au/Ti composite films at various temperatures * [from ref 10]

4.5.3 Surface Topography

Figure 63 shows a summary of SEM micrographs of Au/Cu, Au/Sn, Au/V, and Au/Ti composite films annealed at 500 °C for 1 hour in air demonstrating the effects of Cu-, Sn-, V-, and Ti- underlays on the stability of gold thin films during isothermal annealing in air.

The following conclusions can be made that (1) Au/Cu composite films form holes in the gold films during annealing in air. The holes in Au/Cu composite films are partially filled with copper oxide (CuO). (2) Au/Sn composite films form neither hillocks nor holes during annealing in air. Au/Sn composite films show a rough surface structure in both as-deposited and annealed composite films results from the rough surface structure of the Sn underlays. This observation is similar to that found for Au/In composite films [10]. (3) Au/V and Au/Ti composite films form hillocks during annealing in air which mainly consist of Au.

4.5.4 Film Texture (Preferred Orientation)

Figure 64 shows X-ray diffraction patterns of as-deposited Au/Cu, Au/V, Au/Ti and Au/Sn composite films. The difference of the film texture is evident in the X-ray diffraction pattern of as deposited Au/Sn compared to that of the other composite films. As has been previously shows the film texture of as-deposited Au/Cu, Au/Sn, Au/V and Au/Ti composite film are retained after annealing regardless of the annealing temperature up to 500 °C.

It is concluded that (1) gold films in as-deposited Au/Cu, Au/V and Au/Ti composite films have a (111) preferred orientation parallel to the substrate surface. The (111) preferred orientation of gold is retained after annealing regardless of the annealing temperature. (2) In contrast, the gold films in as-deposited Au/Sn have a

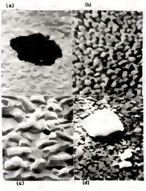

Figure 63 Scanning electron micrographs of gold composite films annealed at 500 °C (60° tilt)

(a) Au/Cu composite films
(b) Au/Sn composite films
(c) Au/V composite films
(d) Au/Ti composite films

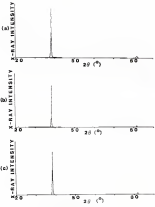

Figure 64 X-ray diffraction patterns of as-deposited gold composite films
(a) Au/Cu composite films
(b) Au/V composite films
(c) Au/Ti composite films
(d) Au/Sn composite films

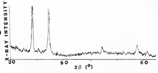

Figure 64 (continued)

random orientation with a slightly stronger (200) orientation parallel to the substrate. The random orientation of gold is retained after annealing regardless of the annealing temperature.

4.5.3 Evolution of Microstructure

Table 3 and Table 4 show the characteristics of the microstructure in as-deposited and in annealed Au/Cu, Au/Sn, Au/V and Au/Ti composite films. Figure 65 schematically depicts the evolution of microstructure in Au/Cu, Au/Sn, Au/V and Au/Ti composite films during annealing in air. It visualizes the effects of Cu-, Sn-, V- and Ti underlays on the stability of gold thin films during isothermal annealing in air by comparing the microstructures of the as-deposited Au/Cu, Au/Sn, Au/V and Au/Ti composite films with those of the composite films annealed at 500 °C for 1 hour in air.

This demonstrates the effects of metal underlays on the stability of gold metallizations in microelectronic circuits. These effects may cause failures during fabrication and during operation of a device.

Table 3 Characteristics of microstructures in as-deposited composite films

System	Surface Topography	Grain Size (Å)	Texture
Au/Co	Smooth	700	111
Au/Sn	Rough	750	Random
Au/V	Smooth	1000	111
Au/Ti	Smooth	3000	111

Table 4 Characteristics of microstructures of gold composite films annealed at 500 °C in air

System	Surface Topography	Grain Size (Å)	Texture
Au/Co	Holes	4100	111
Au/Sn	Rough	1400	Random
Au/V	Hillocks	2700	111
Au/Ti	Hillocks	1200	111

The Evolution of Microstructure

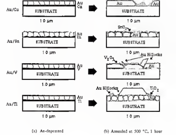

(a) As-deposited

(b) Annealed at 500 °C, 1 hour

Figure 65 The evolution of microstructure in gold composite films during annealing in air.

CHAPTER 5
FURTHER DISCUSSIONS

5.1 Formation of Holes and Hillocks in Gold Composite Films

The formation of holes and hillocks during annealing has been reported in various thin films under a wide range of condition. It goes without saying that holes and hillocks are detrimental during the performance of a microelectronic device causing electrical opens and shorts in integrated circuits. It is suggested from the present annealing study that the following factors may be critical for the reliability of gold metallizations in microelectronic devices.

5.1.1 Thermal Stress in Gold Films Induced by Metal Underlays During Annealing

The mechanisms of hole and hillock formation in gold composite films with rising temperatures are probably very complex because of the multilayer film geometry and because of the out-diffusion of the underlay metals which continuously change the film geometry and composition during annealing. One of the mechanisms which might contribute to hole and hillock formation is thermal stress. This will be discussed at first. Thermal stress can be introduced by the difference in the thermal expansion coefficients between gold and underlay metals. For the following discussion we assume: (a) that the underlay and the gold film have an equal shape (b) a biaxial (two dimensional) system of stress in the films (c) that an equal amount of stress in the x and y direction is applied (d) that the isotropic elasticity theory is valid, (e) that the films are strongly bonded to each other at their common interface (f) for the time being the interactions between metal underlay and the SiO_2 substrate are neglected. This can be done when the underlay metals do not adhere well to the substrates. Indeed, our experiments have shown that when a self-sticking tape is shortly pressed on a Au/Cu composite film which was deposited on a quartz glass substrate, both metal films can be easily and simultaneously lifted off from the substrate when removing the tape. This removal of the composite metal film is even more complete after annealing which suggests a weak adhesion between the metal films and the substrate.

As has been derived in Chapter 2, the thermal stress σ_{th}, in a gold film during annealing is given by

$$\sigma_{th} = \{E_f E_M/(1-\nu)(E_f + E_M)\}(\alpha_f - \alpha_M)(Ta - Ts)$$

where E_f = the Young's modulus of the gold film

E_M = the Youngs modulus of the underlay metal

ν = the Poisson's ratio

α_f = the thermal expansion coefficients of the gold film

α_M = the thermal expansion coefficients of the underlay metal

Ta = the annealing temperature

Ts = the substrate temeprature during deposition

Table 5 gives thermal expansion coefficients, Young's moduli and some other physical constants of the materials used in this study, taken from several sources [145-149]. For many materials the Poisson's ratio (ν) can be taken to be 0.25 [150]. Using these values and assuming the substrate temperature during deposition Ts = 45 °C [90], then the thermal stress during annealing at 500 °C can be calculated by the above equation. Table 6 shows the calculated thermal stress in gold films

Table 5 Physical constants of selected materials (from ref [145-149])

Material	Atomic No	Atomic Weight	Density (g/cm ^{3}) at 20 °C	Melting Point °C	Youngs Modulus (E) (10^6 psi) at 25 °C	Thermal Exp Coeff (10^{-6} °C)
Au	79	197.0	19.32	1063	11.6	14.2
Cu	29	63.54	8.96	1083	17	16.5
Sn	50	118.70	7.30	231.9	6	23
In	49	114.82	7.31	156.2	1.6	33
V	23	50.94	6.1	1900	19	8.3
Ti	22	47.90	4.51	1668	16.8	8.41
SiO_2					45	0.55

Table 6 Calculated thermal stress in gold films induced by metal underlays during annealing at 500 °C assuming that (a) the underlays and the gold film have an equal shape and an equal thickness and (b) the interactions between the metal underlay and the SiO_2 substrate are neglected

$\sigma_{th} = \{ E_{Au}E_{metal}/(1-\nu)(E_{th} + E_{metal}) \} (\alpha_{metal} - \alpha_{Au}) (Ts-Ta)$

Gold Composite Films	Thermal Stress, $\sigma_{th}(10^{10}$ psi), in Gold
Au/Co	1.0 (tensile stress)
Au/Sn	2.1 (tensile stress)
Au/V	-2.6 (compressive stress)
Au/Ti	-2.4 (compressive stress)

* $\sigma_{y\text{-}Au}$ is approx 3.0×10^4 psi

induced by the different thermal expansion coefficients between gold and the underlay metals. A positive value for σ_{th} corresponds to a tensile stress in the gold film. The calculated thermal stress in gold films is much larger than the yield strength of gold, $\sigma_{y\,Au} = 3.0 \times 10^4$ psi [151]. It is thus not unreasonable to consider that gold films may deform plastically for stress relaxation resulting in the formation of holes or hillocks.

As stated in Chapter 2, a diffusion induced flow of matter may be caused by a concentration gradient of vacancies between differently stressed boundaries in a polycrystalline solid [35-37]. In the absence of pressure gradients the flux of atoms, due to the migration of lattice vacancies or interstitial atoms, will be proportional to the gradient of the concentration of these lattice defects. In the presence of pressure gradients, however, it tends to be energetically advantageous to move the lattice defects in whichever direction will relieve the inequality of pressure [35]. The atom flow will be opposite to the vacancy flow causing the grains to elongate in the direction of tensile stress.

In thin films under biaxial stress, this concentration gradient is present between grain boundaries parallel and perpendicular to the free surface [25]. Figure 66 schematically shows the mass transport in gold films by thermal stress induced by the difference in thermal expansion coefficients between gold and an underlay metal during annealing. (As above, the influence of the substrate is neglected.) The mass transport occurs from the free surface into the interior of the gold films for tensile stress and it occurs from the interior onto the free surface of the gold films for a compressive stress resulting in the formation of holes (or grooves) and hillocks in gold films, respectively.

In Au/Cu composite films the difference in thermal expansion coefficients between gold and copper results in a tensile stress during annealing as shown in Table 6. It is thus expected that the mass transport in gold films occurs from the free surface into the interior of gold films resulting in the formation of holes in gold films as shown in Figure 66a.

In Au/V and Au/Ti composite films, however, the difference in thermal expansion coefficients between gold and underlay metals (vanadium and titanium, respectively) results in a compressive stress during annealing as shown in Table 6. Thus the mass transport in gold films is expected to occur from the interior onto the free surface of gold films possibly resulting in the formation of hillocks on the free surface of gold films as shown in Figure 66b.

By inspecting Table 5, it is noticed that the expansion coefficients of V, Ti, and SiO_2 are all smaller than that of Au. Consequently, the influence of stress of V and Ti on the gold film is in the same direction as that of the SiO_2 substrate (compressive) irrespective of the adhesion of V and Ti on SiO_2 (which is actually quite good).

These considerations correspond to the experimental findings reported in Chapter 4. It is thus believed that the formation of holes in Au/Cu composite films and the formation of hillocks in Au/V and Au/Ti composite films are at least in part associated with a stress relaxation phenomenon. Tensile stress in gold films promotes the formation of holes, while compressive stress causes hillocks during annealing.

It should be noted that when the films are completely bonded to the substrate, the thermal expansion coefficient of the SiO_2 substrate is dominant for

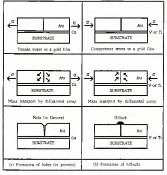
σ
Au
σ
Cu
SUBSTRATE
Tensile stress in a gold film
σ
Au
σ
V or Ti
SUBSTRATE
Compressive stress in a gold film
σ
Au
σ
Cu
SUBSTRATE
Mass transport by diffusional creep
σ
Au
σ
V or Ti
SUBSTRATE
Mass transport by diffusional creep
Hole (or Groove)
Au
Cu
SUBSTRATE
Hillock
Au
V or Ti
SUBSTRATE
(a) Formation of holes (or grooves)
(b) Formation of hillocks

Figure 56 Mass transport by diffusional creep in gold composite films
(a) formation of holes (or grooves)
(b) formation of hillocks

the thermally induced stress in the films irrespective of the expansion coefficient of the underlay. This would result in a compressive stress in gold films during annealing for all types of underlays. However it has been reported that the noble metals, silver, copper, gold, do not adhere well to SiO_2 and tend to ball up during annealing [17]. This observation has been used in the above mentioned considerations.

It is interesting to note in this context that a tensile stress in Au/Sn composite films (Table 6) would predict the formation of holes in gold films as in Au/Cu composite films. However, Au/Sn composite films form neither hillocks nor holes during annealing in air. This is believed to be due to the following characteristics of Au/Sn composite films: (a) as-deposited Au/Sn composite films form already a thin tin oxide layer on the free surface of gold without annealing. (b) the Au/Sn composite films show a rough surface structure in both, as-deposited and in annealed composite films, which results from the rough surface structure of the Sn underlays. The beneficial effects of surface oxide layer and rough surface structure on the stability of gold thin films have been also observed in Au/In gold composite films [3, 10].

5.1.2 Volume Change due to the Formation of Oxides of the Underlay Metals

As previously discussed in Chapter 4, Cu, Sn, V and Ti underlays sandwiched between gold thin films and substrate form oxides (CuO, SnO_2, V_2O_5 and TiO_2, respectively) on the free surface of gold and along the grain boundaries of the gold films during annealing in air.

The formation of oxides is concomitant with a volume increase during annealing in air. Assuming that a metal underlay of 130 Å thickness has been completely oxidized and formed an oxide layer, the thickness of the oxide layer per unit area can be estimated by [152]

$$t_{ox} = A (d_M/d_{ox})(W_{ox}/W_M) \times t_M$$

where t_{ox} = thickness of the oxide, d_M, d_{ox} = density of the underlay metal and its oxide, respectively, W_M, W_{ox} = molecular weight of the metal underlay and its oxide, respectively, and A= 1 for the chemical reactions. (1) $Cu + 1/2\ O_2 = CuO$; (2) $Sn + O_2 = SnO_2$; (3) $Ti + O_2 = TiO_2$, and A=1/2 for the chemical reaction. $2V + 5/2 O_2 = V_2O_5$. Table 7 shows the increase of the thickness per unit area due to the formation of oxides calculated by the above equation.

There may be a correlation between the volume increase due to the formation of oxides and the volume of hillocks formed on the free surface of gold films in Au/V and Au/Ti composite films during annealing in air. Table 8 shows some characteristics of hillocks observed in Au/V and Au/Ti composite films during annealing in air. About 77% of the film surface was covered with "columnar" hillocks in Au/V composite films annealed at 500 °C while about 6% of the film surface was covered with "plate" hillocks in Au/Ti composite films annealed at 500 °C. The average height of hillocks was about 200 Å in Au/V and about 1400 Å and Au/Ti composite films. In other words a small hillock height goes concomitant with large area fraction (and vice versa).

Let us consider a circular cell of gold films as shown in Figure 67. Let the

unit area of gold film (A) = 1 $\mu m^2 = 10^8$ Å^2
thickness of gold film(t) = 750 Å, and
volume of gold film (V) = A•t = 7.5 x 10^{10} Å^3.

Table 7 Increase of the thickness due to the formation of oxides $t_{ox} = A(d_M/d_{ox})(W_M/W_{ox}) \times t_M$, assuming that all the underlay metals have been completely oxidized

Chemical Reactions	Thickness per unit area (Å)
$Cu + 1/2\,O_2 = CuO$	130 (Cu) ----> 220 (CuO)
$Sn + O_2 = SnO_2$	130 (Sn) ----> 270 (SnO_2)
$2V + 5/2\,O_2 = V_2O_5$	130 (V) ----> 320 (V_2O_5)
$Ti + O_2 = TiO_2$	130 (Ti) ----> 230 (TiO_2)

Table 8 Characteristics of hillocks in Au/V and in Au/Ti composite films during annealing

Characteristics	Annealed at 500 °C	
	Au/V	Au/Ti
Shape of Hillocks	"columnar" hillock	"plate" hillock
Average Height of Hillocks	about 200 Å	about 1400 Å
Area Fraction of Hillocks, %	77 % ± 4% (2 S.E.)	6 % ± 1% (2 S.E.)

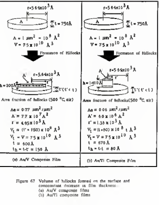

Figure 67 Volume of hillocks formed on the surface and concomitant decrease in film thickness
(a) Au/V composite films
(b) Au/Ti composite films

Taking the values in Table 8, the volume of hillocks (V') formed on the free surface of gold films, the total volume of the system (V_t), and the thickness of the gold films (t') after the formation of hillocks during annealing is given by

(a) Au/V composite films

$V' = Aa \cdot h = 150 \times 10^8$ (Å^3)

where Aa = area fraction of hillocks and

h = average height of hillocks,

$V_t = A \cdot t' + Aa \cdot h = (t' + 150) \times 10^8$ (Å^3), and

$V = V_t = 750 \times 10^8$ (Å^3), ∴ $t' = 600$ (Å)

(b) Au/Ti composite films

$V' = Aa \cdot h = 80 \times 10^8$ (Å^3),

$V_t = A \cdot t' + Aa \cdot h = (t' + 80) \times 10^8$ (Å^3), and

$V = V_t = 750 \times 10^8$ (Å^3) ∴ $t' = 670$ Å

Assuming a conservation of total volume of the system yields V=V'. Thus the thickness of the gold films, t, will decrease and becomes t' = 600 Å due to the formation of hillocks on the free surface of gold films in Au/V composite films annealed at 500 °C. Similarly, t' is 670 Å for annealed Au/Ti films.

The decrease in thickness of the gold films ($t_h = t - t'$) will be 150 Å and 80 Å in Au/V and Au/Ti composite films, respectively. This is due to the formation of hillocks on the surface of the gold films during annealing. Thus the total volume of hillocks (V') are 150×10^8(Å^3) and 80×10^8(Å^3) in Au/V and Au/Ti composite films, respectively.

From Table 7, the volume increase, $V_{oxide} - V_{metal}$, due to the formation of oxides of the underlay metals will become theoretically about 190×10^8 (Å^3) and

100 x 10^8 ($Å^3$) per unit area (1 μm^2 = 10^8 $Å^2$) in Au/V and Au/Ti composite films respectively.

Compared to Au/Cu and Au/Sn composite films, Au/V and Au/Ti composite films are believed to form a substantial amount of oxides of underlay metals along the grain boundaries of the gold films during annealing as shown in Figure 68. Assuming that all oxides form along the gold grain boundaries in Au/V and Au/Ti composite films during annealing, then the total volume of the hillocks (V) formed on the surface of the gold films becomes approx. 80% of the volume increase, V_{oxide}- V_{metal}, due to the formation of oxides of the underlay metals in both Au/V and Au/Ti composite films.

Thus the total volume of hillocks formed on the surface of gold films is proportional to the volume increase of the oxides of the underlay metals which form along the grain boundaries of the gold films. This suggests that the volume increase due to the formation of the internal oxides of the underlay metals can be a possible force for the growth of hillocks during annealing.

5.1.3 Surface Energy

Another mechanism for hole formation in gold films is through capillarity forces. This will be explored now. Previous work [10] has shown that pure gold films form grain boundary grooves (also called thermal grooves) during annealing. Thermal grooving is caused by a mass transport due to an imbalance of surface tension where grain boundaries meet the free surface [3-5, 10]. It was suggested by Srolovitz et al. [40] that the ratio of hole diameter to the mean grain diameter, $\rho = d_0/D$ must be greater than $\rho_{min} = (\sqrt{\Gamma} - \Gamma) / (1 - \Gamma)$ where $\Gamma = 3\gamma_{gb}/2\pi\gamma_v$ (γ_{gb} = grain boundary energy and γ_v = film surface energy)

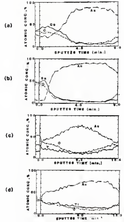

Figure 68 Auger sputter profiles of gold composite films annealed at 500 °C for 1 hour in air.
(a) Au/Cu composite films
(b) Au/Sn composite films
(c) Au/V composite films
(d) Au/Ti composite films

According to the interfacial free energy data [153], the average values of γ_{gb} and γ_v for gold can be obtained by

$$\gamma_{gb}\ (J/m^2) = -1.0 \times 10^{-4}T + 0.478,$$

$$\gamma_v\ (J/m^2) = -4.3 \times 10^{-4}T + 1.830$$

The mean grain diameter of gold in Au/Cu composite films annealed at 500 °C is about 4000 Å (Chapter 4).

Using the values of D=4000 Å, γ_{gb}=0.428 J/m^2 and γ_v=1.615 J/m^2 for gold at 500 °C, Γ is 0.13 and therefore $\rho_{min.}$ becomes 0.27. The surface energy argument thus predicts that the hole size in annealed gold films should be larger than 0.1 μm in diameter when the mean grain diameter of gold is 4000Å. The hole sizes were experimentally found to vary between 0.2 and 1.5 μm in diameter when Au/Cu composite films were annealed at 500 °C for 1 hour in air (Chapter 4). This suggests that capillarity force (surface tension) may also contribute to the formation and growth of holes in Au/Cu composite films during annealing.

5.1.4 Oxidation Tendency of the Underlay Metals

Figure 69 shows the oxidation tendency of selected materials (Richardson's Diagram) and SEM micrographs of Au/Cu, Au/Sn, Au/V and Au/Ti composite films annealed at 500 °C. It is noted that (1) Au/Cu (and also Au/Ni [13-14]) composite films (small oxidation tendency of the underlay metal) form holes; (2) Au/Sn (and also Au/In [3,10]) composite films (moderate oxidation tendency of the underlay metal) form a rough surface structure and form neither holes nor hillocks; (3) Au/V and Au/Ti composite films (strong oxidation tendency of the underlay metal) form hillocks during annealing in air.

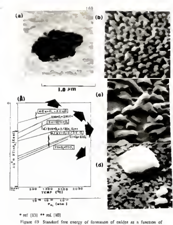

* ref [13] ** ref. [10]

Figure 69 Standard free energy of formation of oxides as a function of temperature (A) and SEM micrographs (a-d) of annealed gold composite films at 500 °C for 1 hour in air (60° tilt)
(a) Au/Cu composite films
(b) Au/Sn composite films
(c) Au/V composite films
(d) Au/Ti composite films

This may suggest that the oxidation tendency of the underlay metals influence the stability of gold thin films during annealing in air. The underlay metals which have a strong tendency towards oxidation are likely to form internal oxides along the grain boundaries of the gold films during annealing. The formation of oxides is concomitant with a volume increase as mentioned above. The volume increase in turn causes extrusions of gold atoms resulting in the formation of hillocks on the free surface of the gold films.

The underlay metals which have a small tendency towards oxidation mainly form surface oxides on top of the gold films during annealing. In this case, the gold films may form holes in gold films by capillarity (surface tension) force during annealing. The underlay metals which have a moderate oxidation tendency towards oxidation form neither holes nor hillocks and form a rough surface structure.

In summary, (1) Tensile stress in gold films promotes the nucleation of hole formation in Au/Cu composite films, while compressive stress causes hillocks in Au/V and Au/Ti composite films during annealing. (2) Capillarity (surface tension) may be a second force for the growth of holes in Au/Cu composite films during annealing; (3) The volume increase due to the formation of the internal oxides of the underlay metals may contribute to the growth of hillocks in Au/V and Au/Ti composite films during annealing.

It is this interplay between stress (caused by the mismatch of thermal expansion coefficients), capillarity forces, and oxidation behavior of the underlay metals what causes the variety of experimental observations reported in this study.

It is concluded from these results that the following factors of metal underlays may be critical for the stability of gold thin films during isothermal annealing in air

A. Oxidation tendency of metal underlays

B. Thermal stress due to the difference in thermal expansion coefficients

C. Volume change due to the formation of oxides of the underlay metals

D. Surface energy

The next step for assessing the suitability of these composite films for microelectronic devices needs to address the electrical properties of gold composite films including their resistivity change and the MTF (Median-Time-To-Failure) under d.c. stressing.

CHAPTER 6
CONCLUSIONS

From the present study on the effects of Cu-, Sn-, V- and Ti underlays on the stability of gold films, the following conclusions can be drawn

1. Oxides
   a. Cu-, Sn-, V- and Ti underlays sandwiched between gold thin films and substrate form oxides (CuO, SnO_2, V_2O_5 and TiO_2, respectively) on the free surface of gold and along the grain boundaries of the gold films during annealing in air
   b. Au/Cu and Au/Sn composite films form more complete and thicker oxide layers (CuO and SnO_2 respectively) on top of gold films during annealing compared to Au/V and Au/Ti composite films.
   c. As deposited Au/Sn composite films form already a thin tin oxide layer on the free surface of gold without annealing, that is, during 30 days storage at room temperature. The thickness of a tin oxide layer increases during annealing between 300 °C and 500 °C for 1 hour in air
2. Grain Growth
   a. The oxides which formed during annealing reduce in most cases the tendency towards growth of the gold grains. This is interpreted to be caused by a capping of the gold surface and by pinning the grain boundaries of the gold films by the oxide

b. Ti underlays which have a strong tendency towards oxidation prevent grain growth of gold during annealing as stated above, while Cu underlays which have a small tendency towards oxidation do not prevent grain growth of gold during annealing

3 Holes/Hillocks

a. In Au/Cu composite films some holes in the gold films are observed which form during annealing for 1 hour in air at temperatures between 300 °C and 500 °C. The holes in Au/Cu composite films are partially filled with copper oxide (CuO).

b. The density of holes in Au/Cu composite films stays nearly constant with annealing time at 400 °C in air, while the area fraction of holes increases with annealing time in a near parabolic manner

c. Au/Sn composite films form neither hillocks nor holes during annealing in air

d. Au/V and Au/Ti composite films form hillocks during annealing in air which mainly consist of Au The volume increase of Au/V and Au/Ti composite film thus obtained is believed to be due to the formation of oxides (V_2O_5 and TiO_2, respectively)

e. It is believed that the formation of holes in Au/Cu composite films and the formation of hillocks in Au/V and Au/Ti composite films are caused by an interplay between stress (caused by the mismatch of thermal expansion coefficients) capillarity forces, and oxidation behavior of the underlay metals

4. Surface Structure
    a. Au/Sn composite films show a rough surface structure in both as deposited and annealed composite films. The surface roughness of Au/Sn composite films results from the rough surface structure of the Sn underlays.
5. Preferred Orientation
    a. The gold films in as deposited Au/Cu, Au/V and Au/Ti composite films have a (111) preferred orientation parallel to the substrate surface. The (111) preferred orientation of gold is retained after annealing regardless of the annealing temperature. In contrast, the gold films in as-deposited Au/Sn composite films have a random orientation with a slightly stronger (200) orientation parallel to the substrate surface. The random orientation of gold is retained after annealing regardless of annealing temperature.

The above listed conclusions demonstrate how metal underlays influence the stability of gold metallizations in microelectronic circuits. They may cause failures during fabrication and during operation of a device. This work has shown that the following factors may be critical for the reliability of gold metalizations in microelectronic devices.

A. Oxidation tendency of metal underlays. In general, a strong tendency towards oxidation of the metal underlay prevents grain growth of gold during annealing. This is probably caused by grain boundary pinning of the metal oxides.

B. Thermal stress due to the difference in thermal expansion coefficients
Tensile stress in gold films promotes the nucleation of hole formation, while compressive stress causes hillocks during annealing

C. Volume change due to the formation of oxides of the underlay metal
The volume increase due to the formation of the internal oxides of the underlay metals may contribute to the growth of hillocks in gold composite films during annealing

D. Surface Energy Capillarity (surface tension) may be a second force for the growth of holes in gold composite films during annealing.

REFERENCES

1. R. E. Hummel, Electronic Properties of Materials, Springer-Verlag Co., New York, 1985, 115
2. R. E. Hummel, Electro- and Thermo-Transport in Metals and Alloys, Amer. Inst. of Mining, Metallurgical and Petroleum Engineers, Inc., New York 1977, 93
3. R. E. Hummel, Application and Deterioration of Thin Films for Microelectronic Devices, in Chemisorption of Gases on Metal Films, Elsevier Science and Publishing Co. Amsterdam New York 1986
4. R. E. Hummel, R. T. DeHoff, S. M. Goho and W. M. Goho, Thin Solid Films, 78, 1981, 1
5. R. E. Hummel, S. M. Goho and R. T. DeHoff, Proc. 22nd Ann. Rel. Phy. Symp. IEEE, 1984, 234
6. R. E. Hummel, B. K. Krumeich and R. T. DeHoff, Appl. Phys. Lett. 33(11), 1978, 960
7. R. E. Hummel, H. J. Geier, Thin Solid Films, 25, 1975, 335
8. R. E. Hummel and R. M. Breitling, Appl. Phys. Lett. 18(9), 1971, 373
9. H. M. Breitling and R. E. Hummel, J. Phys. Chem. Solids, 33, 1972, 845
10. S. Y. Lee, R. E. Hummel and R. T. DeHoff, Thin Solid Films, 149, 1987, 29
11. F. O. Sequeda, Journal of Metals, 37(5), 1985, 43
12. F. O. Sequeda, Journal of Metals, 17(11), 1985, 54
13. Y. K. Chao, S. K. Kurinec, I. Toor, H. Shillingford and P. H. Holloway, J. Vac. Sci. Technol. A5(3), 1987, 337

14 S K Kurinec, I Toor, Y K Chao, H Shillingford, and P H Holloway, S Ray, and K Beckham, Intl Symp on Hybrid Microelectronics, Atlanta, Oct., 1986

15 J R. Black IEEE Trans. Electron Devices, ED-16, 1969, 338

16. R. E Hummel, R. T DeHoff and H. J Geier, J Phys. Chem. Solids, 37, 1976, 73

17 M A. Nicolet Thin Solid Films 52, 1978 415

18 P H. Holloway and C C Nelson, Thin Solid Films, 35, 1976, L13

19 J Raloff, Science News, 134(3), 1988, 33

20 F D Richardson and J H E Jeffes, J Iron Steel Inst 160 1948 261

21 D A. Porter and K. E. Eastering, Phase Transformations in Metals and Alloys, Van Nostrand Reinhold (UK) Co. Ltd Berkshire, 1981, 130

22 H Hu Metals Handbook, Vol. 9, Metallography and Microstructures, ASM, Metals Park Ohio 1985, 692

23 K L. Chopra, Thin Film Phenomena, Krieger Publishing Co , New York, 1979, 272

24 A E S Presland, G L Price and D L. Trimm Surface Science 29, 1972, 424

25 P Chaudhari, IBM J Res Develop 13, 1969, 197

26. S Timoshenko and J N Goodier, Theory of Elasticity, McGraw Hill Book Co., Inc, New York, 1951, 399

27 K. L Chopra, Thin Film Phenomena, Krieger Publishing Co., New York 1979, 271

28 V M Koleshko, V F Belitsky and I V Kiryushin, Thin Solid Films, 142, 1986 199

29 M Hershkovitz, I A Blech, and Y Komem, Thin Solid Films, 130 1985, 87

30 P Chaudhari J Appl Phys 45(10) 1974, 4339

31 P Chaudhari, IBM Res Rep., 1974, RC4780

32 G E. Dieter, Mechanical Metallurgy McGraw Hill Inc , New York, 1976, 72

33 S K. Groothuis, Texas Instruments Res Rep. 1988 RADC-TR 88 8

34 S K. Groothuis and W Schroen, Proc 25th Ann Rel Phy Symp IEEE, 1987, 1

35 C Herring, J Appl Phys 21, 1950, 437

36 R L. Coble J Appl. Phys 34(6) 1963, 1679

37 G B Gibbs Phil Mag. 13 1966 589

38 M F Ashby Acta Met 20, 1972 887

39 T Turner and K Wendel, Proc 23rd Ann Rel Phy Symp IEEE, 1985 142.

40 D J Srolovitz and S A Safran, J Appl Phys, 60(1), 1986, 247

41 D J Srolovitz and S A Safran, J Appl Phys 60(1), 1986, 255

42. J T Yue, W F Funsten, and R. V Taylor Proc. 23rd Ann Rel Phy Symp IEEE, 1985, 126

43 J R Lloyd and S Nakahara Thin Solid Films, 93, 1982, 281

44 J R. Lloyd and S Nakahara, J Electrochem. Soc 125(12), 1978, 2037

45 J R Lloyd and S Nakahara, J Appl Phys. 48(12), 1977, 5092

46 J R. Lloyd and S Nakahara Thin Solid Films, 45, 1977, 411

47 J R. Lloyd and S Nakahara, J Vac. Sci Technol, 14(1), 1977, 655

48 S Nakahara, Thin Solid Films, 64 1979, 149

49 S K Sharma and J Spitz, JEOL News 20E(2), 1982, 22(49)

50 S K Sharma and J Spitz, Thin Solid Films, 67, 1980, 109

51 S K Sharma and J Spitz, Thin Solid Films, 65, 1980, 339

52 S K Sharma and J Spitz, Thin Solid Films 56 1979 L17

53 A. E S Presland G L Price and D L. Trimm, Surface Science, 29, 1972, 435

54 S Nakahara and R J McCoy Thin Solid Films 88 1982, 285

55 S Nakahara and R. J McCoy, Appl Phys Lett., 37(1), 1980, 42

56 J R Lloyd and S Nakahara, Thin Solid Films, 54, 1978, 207

57 H C W Huang Appl Phys Lett. 41(8), 1982, 724

58 L. G. Feinstein and J. B. Bindell, Thin Solid Films, 62, 1979, 37

59 M. R. Pinnel and J. E. Bennett, Met. Trans., 3, 1972, 1989

60 M. R. Pinnel and J. E. Bennett, Met. Trans. (A), 7(A), 1976, 629

61 F. Seitz, Acta Met., 1, 1953, 355

62 R. W. Balluffi, Acta Met., 2, 1954, 194

63 J. A. Brinkman, Acta Met., 3, 1955, 140

64 K. Hinode, N. Owada, T. Nishida and K. Mukai, J. Vac. Sci. Technol. B5(2), 1987, 518

65 S. Mayumi, T. Umemoto, M. Shishino, H. Nanatsue, S. Ueda, and M. Inoue, Proc. 25th Ann. Rel. Phy. Symp. IEEE, 1987, 15

66 A. D. Smigelskas and E. D. Kirkendall, Trans. AIME, 171, 1947, 130

67 W. M. Kane, J. P. Spratt and L. W. Hershinger, J. Appl. Phys., 37(5), 1966, 2085

68 M. L. Gimple, A. D. McMaster and N. Fuschillo, J. Appl. Phys., 15(12), 1964, 3572

69 S. J. Harris and E. C. Darby, Gold Bull., 9(3), 1976, 81

70 C. J. Raub, H. R. Khan and J. Lendvay, Gold Bull., 9(4), 1976, 123

71 D. S. Herman, M. A. Schuster and R. M. Gerber, J. Vac. Sci. Technol., 9(1), 1972, 515

72. S. K. Lahiri and O. C. Wells, Appl. Phys. Lett., 15(7), 1969, 234.

73 C. J. Santoro, J. Electrochem. Soc., 116(3), 1969, 361

74 F. d'Heurle, L. Berenbaum and R. Rosenberg, Trans. AIME, 242, 1968, 502

75 W. B. Pennebaker, J. Appl. Phys., 40(1), 1969, 394

76 R. L. Schwoebel, J. Appl. Phys., 37, 1966, 2515

77 S. K. Lahiri, J. Appl. Phys., 41(7), 1970, 3172.

78 S. K. Lahiri, J. Appl. Phys., 46(6), 1975, 2791

79 M. Murakami and T. S. Kuan, Thin Solid Films, 66, 1980, 381

80. S. K. Sharma, S. U. M. Rao and N. Kumar, Thin Solid Films, 142, 1986, L95

81. K. Arai and T. Wako, Thin Solid Films, 142, 1986, 139

82. R. Halmi, E. M. Chplievski, D. A. Gorbatchevski, and A. Yazitchenko, Thin Solid Films, 150, 1987, 357

83. H. Y. Yang and X. A. Zhao, J. Vac. Sci. Technol. A, 6(3), 1988, 1646.

84. P. Chaudhari, J. Vac. Sci. Technol., 9(1), 1972, 520

85. A. J. Griffin JR., and F. R. Brotzen, Thin Solid Films, 150, 1987, 237

86. M. Murakami, Acta Met., 26, 1978, 175

87. A. Gangulee, Acta Met., 22, 1974, 177

88. M. F. Ashby, Acta Met., 20, 1972, 887

89. K. L. Chopra, Thin Film Phenomena, Krieger Publishing Co., New York, 1979, 61

90. S. Y. Lee, Ph.D. Dissertation, University of Florida, 1985, 19

91. R. W. Berry, P. M. Hall, and M. T. Harris, Thin Film Technology, Krieger Publishing Co., New York, 1979, 23

92. K. L. Chopra, Thin Film Phenomena, Krieger Publishing Co., New York, 1979, 19

93. M. V. Heimendal, Electron Microscopy of Materials, Academic Press, Inc., New York, 1980, 98

94. L. E. Davis, N. C. MacDonald, P. W. Palmberg, G. E. Riach, and R. E. Weber, Handbook of Auger Electron Spectroscopy, Perkin Elmer Corporation, Eden Prairie, Minnesota, 1978, 15

95. C. D. Wagner, W. M. Riggs, L. E. Davis, J. F. Moulder, and G. E. Muilenberg, Handbook of Xray Photoelectron Spectroscopy, Perkin-Elmer Corporation, Eden Prairie, Minnesota, 1979, 9

96. K. L. Chopra, Thin Film Phenomena, Krieger Publishing Co., New York, 1979, 185

97. H. W. Werner, The Application of Beam and Diffraction Techniques to Thin Film and Surface Micro Analysis, in Thin Film and Depth Profile Analysis, Springer-Verlag Co., New York, 1984, 9

98. H J Mathieu, Depth Profile and Interface Analysis of Thin Films by AES and XPS, in Thin Film and Depth Profile Analysis, Springer Verlag Co., New York 1984, 40

99. G A. Somorjai, Chemistry in Two Dimensions, Surfaces, Cornell University Press, Ltd., New York, 1981, 41

100. J I Goldstein, D E Newbury, P Echlin, D C Joy, C. Fiori, and E. Lifshin, Scanning Electron Microscopy and X ray Microanalysis, Plenum Press, New York, 1981, 44

101. J I Goldstein, D E Newbury, P Echlin, D C Joy, C. Fiori, and E. Lifshin, Scanning Electron Microscopy and X ray Microanalysis, Plenum Press, New York 1981, 92

102. H G Tompkins and M R Pinnel J Appl Phys., 47(9), 1976, 3804

103. M. R. Pinnel, H G Tompkins and J A. Augis, Microstructural Science, Volume 8, Elsevier North Holland Inc., New York 1980, 14

104. M. R. Pinnel, H G Tompkins and D E Heath, Applications of Surface Science, 2(4), 1979, 558

105. M. R. Pinnel, H G Tompkins and D E. Heath, J Electrochem Soc., 126(10), 1979, 1798

106. K. L. Chopra, Thin Film Phenomena, Krieger Publishing Co., New York, 1979, 23

107. C D Wagner, W M. Riggs, L E. Davis, J P Moulder and G E. Muilenberg, Handbook of X ray Photoelectron Spectroscopy, Perkin Elmer Corporation, Eden Prairie, Minnesota, 1979, 82

108. G A Somorjai, Chemistry in Two Dimensions, Surfaces, Cornell University Press, Ltd., New York, 1981, 27

109. G A Somorjai, Chemistry in Two Dimensions, Surfaces, Cornell University Press, Ltd., New York, 1981, 353

110. CRC Handbook of Chemistry and Physics, 63rd ed., CRC Press, Inc., Boca Raton, Florida, 1982 1983, D-101

111. D R Gaskel, Introduction to Metallurgical Thermodynamics, McGraw-Hill Kogakusha Ltd., Scripta Publishing Co., Tokyo 1973, 259

112. M. Hansen, Constitution of Binary Alloys, McGraw Hill Book Co., New York, 1958, 199

113 M. R. Pinnel and J. E. Bennett, Met. Transactions A, 10(A), 1979, 741.

114 B. D. Cullity, Elements of X-ray Diffraction, Addison-Wesley Publishing Co., Reading, MA, 1978, 304.

115 J. R. White, Thin Solid Films, 22, 1974, 23.

116 K. L. Chopra, Thin Film Phenomena, Krieger Publishing Co., New York, 1979, 220.

117 W. L. Winterbottom and N. A. Gjostein, Acta Met., 14, 1966, 1041.

118 J. H. Holomon and D. Turnbull, Prog. Met. Phys., 4, 1953, 333.

119 S. Y. Lee, Ph.D. Dissertation, University of Florida, 1985, 32.

120 N. Mancini and E. Rimini, Surf. Sci., 22, 1970, 357.

121 R. A. Powell, Appl. Surf. Sci., 2, 1979, 397.

122 D. A. Asbury and G. B. Hoflund, J. Vac. Sci. Technol. A 5(4), 1987, 1132.

123 L. E. Davis, N. C. MacDonald, P. W. Palmberg, G. E. Riach, and R. E. Weber, Handbook of Auger Electron Spectroscopy, Perkin-Elmer Corporation, Eden Prairie, Minnesota, 1978, 159.

124 C. D. Wagner, W. M. Riggs, L. E. Davis, J. F. Moulder, and G. E. Muilenberg, Handbook of X-ray Photoelectron Spectroscopy, Perkin-Elmer Corporation, Eden Prairie, Minnesota, 1979, 118.

125 M.Hansen, Constitution of Binary Alloys, McGraw Hill Book Co., New York, 1958, 233.

126 L. Buene, Thin Solid Films, 47, 1977, 159.

127 L. Buene, Thin Solid Films, 43, 1977, 285.

128 A. S. Nowick and J. J. Burton, Diffusion in Solids, Academic Press, Inc., New York, 1975, 224.

129 B. P. Dyson, J. Appl. Phys. 37, 1966, 2375.

130 D. A. Porter and K. E. Easterling, Phase Trasformation in Metals and Alloys, Van Nostrand Reinbold (UK) Co. Ltd. Berkshire, England, 1983, 66.

131 H. G. Tompkins and M. R. Pinnel, J. Appl. Phys., 48, 1977, 3144.

132 P R Underhill Surf int. Anal 8, 1986, 61

133 S S Chan, J Gonzalez-Hernandez, D Martin, and R Tsu, Appl. Phys. Lett. 46(11), 1985, 1089

134 L. E. Davis, N C. MacDonald, P W Palmberg, G E. Riach, and R. E. Weber, Handbook of Auger Electron Spectroscopy, Perkin-Elmer Corporation, Eden Prairie, Minnesota 1978, 75

135 C. D Wagner, W M Riggs, L. E Davis, J F Moulder, and G E Muilenberg, Handbook of X-ray Photoelectron Spectroscopy, Perkin Elmer Corporation Eden Prairie, Minnesota, 1979,70

136 R Pretorius, J M Harris and M A Nicolet, Solid-State Electron., 21, 1978 667

137 K L. Chopra, Thin Film Phenomena, Krieger Publishing Co New York, 1979 321

138 D R Gaskel, Introduction to Metallurgical Thermodynamics, McGraw Hill Kogakusha, Ltd Scripta Publishing Co. Tokyo 1973 102

139 M. Hansen, Constitution of Binary Alloys, McGraw-Hill Book Co., New York, 1958, 241

140 L. E Davis, N C MacDonald, P W Palmberg, G E. Riach, and R E Weber, Handbook of Auger Electron Spectroscopy, Perkin Elmer Corporation Eden Prairie Minnesota, 1978, 73

141 B J Burrow, A E. Morgan and R C. Ellwanger, J Vac Sci Technol A4(6), 1986, 2463

142 C D Wagner W M Riggs L E. Davis, J F Moulder and G E Muilenberg Handbook of X-ray Photoelectron Spectroscopy, Perkin Elmer Corporation, Eden Prairie, Minnesota, 1979 68

143 E. Ritter J Vac Sci Technol 3, 1966 225

144 M Hansen, Constitution of Binary Alloys, McGraw-Hill Book Co., New York, 1958, 238

145 W E Beadle, J C C, Tsai, and R D Plemmer Quick Reference Manual for Silicon Intergrated Circuit Technology, Johe Wiley & Sons Inc New York, 1985, 1-11

146 C R Barrett and A S Tetelman The Principles of Engineering Materials, Prentice Hall Inc., Englewood Cliffs, New Jersey, 1973 540

147 L. H. Van Vlack, Materials Science for Engineers, Addison Wesley Publishing Co., London 1971, 513

148 G. V. Samsonov, The Oxide Handbook, Plenum Data Corporation, New York, 1973, 125.

149 R. E. Hummel, Electronic Properties of Materials, Springer Verlag, New York, 1985, 312.

150 S. Timoshenko and J. N. Goodier, Theory of Elasticity, McGraw Hill Book Co., Inc, New York, 1951, 7.

151 Metals Handbook, Vol. 2, Properties and Selection of Nonferrous Alloys and Pure Metals, 9th ed., American Society for Metals (ASM), Metals Park, Ohio, 1979, 679.

152 S. Y. Lee, Ph.D. Dissertation, University of Florida, 1985, 80.

153 L. E. Murr, Interfacial Phenomenon in Metals and Alloys, Addison Wesley Publishing Co., 1975, 130.

BIOGRAPHICAL SKETCH

Jin Young KIM was born 15 October 1956 in Seoul, Korea. He received a B.S. and a M.S. degree in ceramic engineering from Seoul National University in 1980 and 1982, respectively. The title of the master thesis was "A Study on the Sintering and Dielectric Properties of $(Pb_{1-x}K_y\square_{x-y})(Zr_{0.56}Ti_{0.44})O_{3-x+y/2}$ Systems." The author was then employed by the Korea Advanced Institute of Science and Technology from 1983 to 1984 as a research scientist. He entered the Department of Materials Science and Engineering at the University of Florida as a graduate student in January 1985 and has pursued the degree of Doctor of Philosophy since that day. The author won first place in the Student Paper Contest, Florida Chapter of the American Vacuum Society (AVS) on February 1988 and was awarded an all expenses paid trip for four days to attend the 35th National Symposium of AVS in October 1988.

The author has been a member of the American Vacuum Society since 1987 and a member of the Electron Microscopy Society of America since 1986.

I certify that I have read this study and that in my opinion it conforms to acceptable standards of scholarly presentation and is fully adequate in scope and quality, as a dissertation for the degree of Doctor of Philosophy.

R. E. Hummel

Rolf E. Hummel, Chairman
Professor of Materials Science
and Engineering

I certify that I have read this study and that in my opinion it conforms to acceptable standards of scholarly presentation and is fully adequate in scope and quality, as a dissertation for the degree of Doctor of Philosophy.

Robert T. DeHoff

Robert T DeHoff
Professor of Materials Science
and Engineering

I certify that I have read this study and that in my opinion it conforms to acceptable standards of scholarly presentation and is fully adequate in scope and quality, as a dissertation for the degree of Doctor of Philosophy.

Paul H Holloway

Paul H Holloway
Professor of Materials Science
and Engineering

I certify that I have read this study and that in my opinion it conforms to acceptable standards of scholarly presentation and is fully adequate, in scope and quality, as a dissertation for the degree of Doctor of Philosophy.

Dorothea E. Burk

Dorothea E. Burk
Associate Professor of Electrical
Engineering

I certify that I have read this study and that in my opinion it confirms to acceptable standards of scholarly presentation and is fully adequate, in scope and quality, as a dissertation for the degree of Doctor of Philosophy.

Timothy J Anderson

Timothy J Anderson
Associate Professor of Chemical
Engineering

This dissertation was submitted to the Graduate Faculty of the College of Engineering and to the Graduate School and was accepted as partial fulfillment of the requirements for the degree of Doctor of Philosophy.

December, 1988

W J Schafer

Dean, College of Engineering

Dean, Graduate School